page intentionally left blank.

4. REVIEW OF NUMERICAL MODELS APPLIED TO MASONRY STRUCTURES

The numerical analysis of unreinforced masonry structures (URM) can be carried out using different methods such as limit analysis, finite element method and the discrete element method [*e.g.* Kappos *et al.* 2002; Lourenço 1996; Page 1978; Pelà 2008; Roca *et al.* 2010]. Another approach consists in idealizing the structure through an equivalent frame where each wall is discretized by a set of masonry panels (piers and spandrels) in which the non-linear response is concentrated [*e.g.* Calderini *et al.* 2009; Galasco *et al.* 2004; Gambarotta and Lagomarsino 1997a; b; Lagomarsino *et al.* 2007; Magenes and Della Fontana 1998]. Masonry is a composite material formed by bricks and mortar joints, which each of them having its own material properties. The mortar is normally weaker and softer than the bricks. However, failure of masonry may involve the crushing and tensile fracturing of masonry units in addition to the fracturing of mortar joints [Stavridis and Shing 2010]. Masonry usually refers to fired brick masonry, while adobe masonry refers to adobe bricks (raw earth).

In comparison to masonry (fired bricks) and reinforced concrete structures, few work have been carried out regarding the numerical modelling of adobe constructions. One of the reasons for the little work is the lack of reliable material properties for representing the adobe material in the inelastic range. [Furukawa and Ohta 2009] and [Cao and Watanabe 2004], for example, modelled adobe modules following a finite element approach (FEM) and a discrete element approach (DEM), respectively.

In this work, a finite element approach is followed for modelling adobe masonry following a micro and macro-modelling technique. Besides, the most relevant masonry modelling works are discussed.

4.1 FROM MICRO-MODELLING TO MACRO-MODELLING

In general, the analysis of masonry structures can be classified according to the order of accuracy [Lourenço 1996], Figure 4.1:

- *detailed-micro modelling*. Bricks and mortar joints are represented by continuum elements, where the unit-mortar interface is represented by discontinuous elements [Ali and Page 1987; Cao and Watanabe 2004; Furukawa and Ohta 2009; Rots 1991].

Any analysis with this level of refinement is computationally intensive and it requires a good well documented representation of the material properties (elastic and inelastic) of the constituents.

- *simplified micro-modelling*. The expanded units are represented by continuum elements, where the behaviour of the mortar joints and unit-mortar interface is lumped in discontinuous elements [Arya and Hegemier 1978; Lotfi and Shing 1994; Lourenco and Rots 1997; Page 1978]. This approach can be compared with the discrete element method, originally proposed by Cundall [1971] in the area of rock mechanics, where a special procedure is used for contact detection and contact force evaluation [Lotfi and Shing 1994].
- *macro-modelling or continuum mechanics finite element*. Bricks, mortar and unit-mortar interface are smeared out in the continuum and the masonry is treated as an isotropic material. This methodology is relatively less time consuming than the previous ones, but still complex because of the brittle material behaviour.

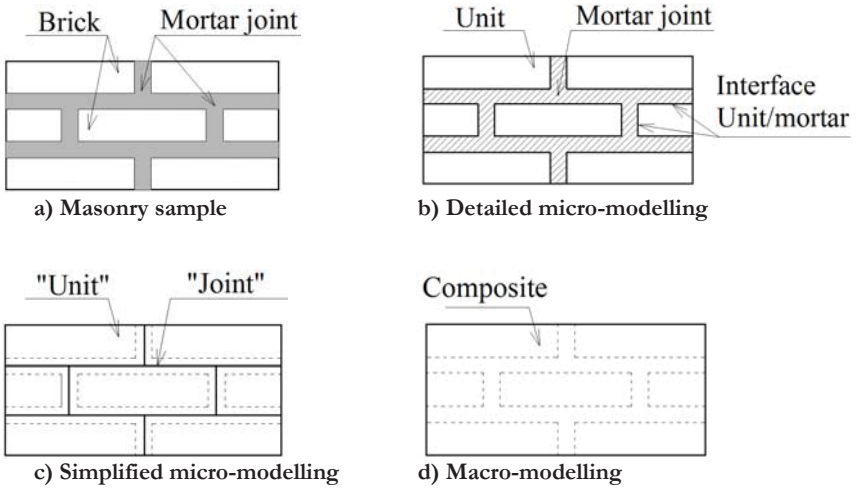

a) Masonry sample **b) Detailed micro-modelling**

c) Simplified micro-modelling **d) Macro-modelling**

Figure 4.1. Modelling strategies for masonry structures (modified from Lourenço [1996]).

The first two approaches are computationally intensive for the analysis of large masonry structures, but they can be an important research tool in comparison with the costly and often time-consuming laboratory experiments [Lotfi and Shing 1994].

The objective in the simplified micro-modelling is to concentrate all the damage in the weak joints and in the potential pure tensile cracks in the bricks, placed vertically in the middle of each brick. According to Lourenço [1996], micro-models are, probably, the best tool available to understand the behaviour of masonry. The benefit of using such an

approach is that all the different failure mechanisms can be considered, mainly: (a) cracking of the joints, (b) sliding along the bed or head joints at low values of normal stress, (c) cracking of the units in direct tension, (d) diagonal tensile cracking of the units at values of normal stress sufficient to develop friction in the joints and (e) "masonry crushing" (Figure 4.2). The (a) and (b) failure mechanisms are joint mechanisms; (c) is a unit mechanism; (d) and (e) are combined mechanisms involving units and joints.

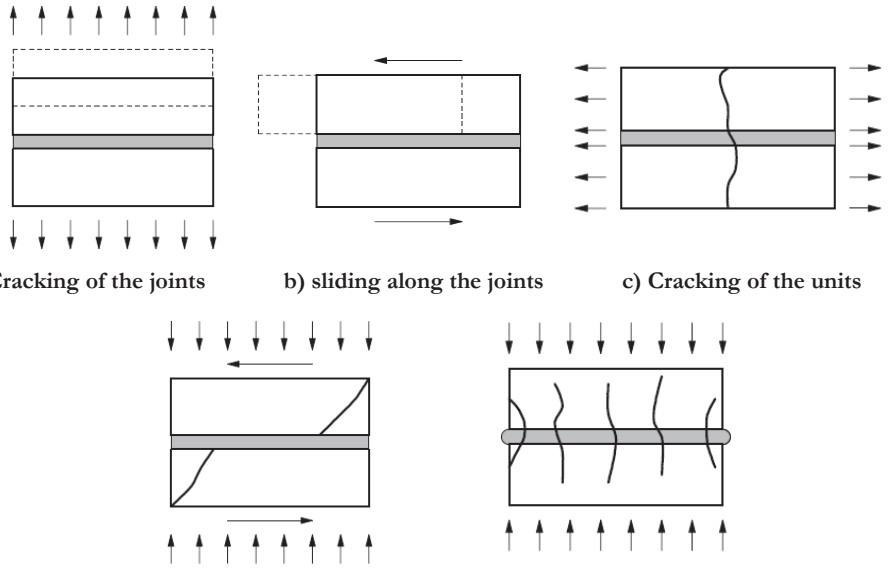

Figure 4.2. Masonry failure mechanisms [Lourenço 1996].

A good approximation of the failure mechanisms for the in-plane loaded masonry walls can be described by the constitutive model developed by Lourenço [1996], which assumes three failure modes: tension cut-off, compression cap, and shear failure, developed under plasticity concepts (Figure 4.3). The internal damage associated with each failure mechanism was modelled in the mortar joints using internal parameters related to fracture energy in tension, compression and shear [Sui and Rafiq 2009].

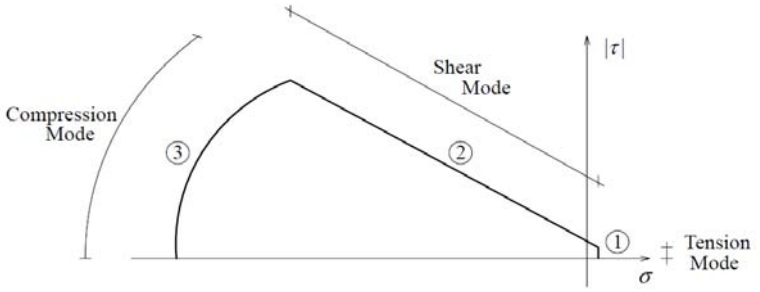

Figure 4.3. Composite yield surface model proposed by Lourenço [1996].

The calibration and validation of Lourenço's constitutive model was based on shear wall tests carried out in Netherlands by CUR [1997] and Raijmakers and Vermeltfoort [1992] on two types of walls: with and without window openings. As follows an explanation of the work presented by Lourenço [1996] for simplified micro-modelling is presented. Four walls without opening (named JD4, JD5, JD5 and JD5) and two with a central opening (named J2G and J3G) were considered for numerical modelling. Each of the tested walls was subjected to a horizontal top displacement, maintaining a given pre-compression force (applied at the top) and maintaining the horizontality of the top beam as shown in Figure 4.4. Pre-compression values of 0.30, 1.21 and 2.12 N/mm² were considered. In the finite element models the bricks were represented by plane stress continuum elements with 8 nodes and the mortar joints by interface elements with 6 nodes. At the middle of each brick an interface element was placed (6 nodes) to simulate potential vertical cracks inside the units (only tension failure was considered in this case).

The experimental crack pattern of the tested walls is shown in Figure 4.5 for compression strength of 0.30 *MPa*. The principal observation was the development of diagonal stepped cracks, simultaneously with cracks in the bricks and crushing of the compressed toes [Raijmakers and Vermeltfoort 1992]. From the numerical model, Lourenço [1996] reports that the collapse mechanism starts with two horizontal tensile cracks concentrated at the top and bottom of the wall, separating the rigid plates from the masonry. Later, a steeped diagonal crack forms cutting mortar and bricks (Figure 4.5). These cracks start at the middle of the wall with crack initiation in the bricks. In the last stage the compressed toes crush and a complete diagonal crack is formed.

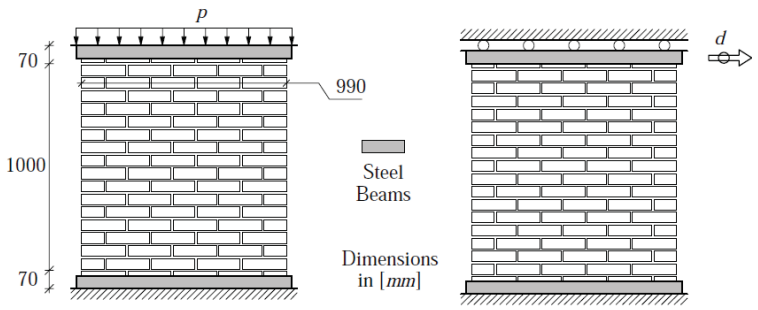

a) Phase 1: vertical loading **b) Phase 2: horizontal loading**

Figure 4.4. Test scheme and sequence of loads of the masonry wall analyzed by Lourenço [1996].

The other type of walls analyzed by Lourenço [1996] considered a central opening. The pre-compression vertical load was 0.30 *MPa*, and similary to the previous case, the horizontal load was applied at the wall top (Figure 4.5). The difference in the numerical models is the absence of vertical interface at the middle of the bricks.

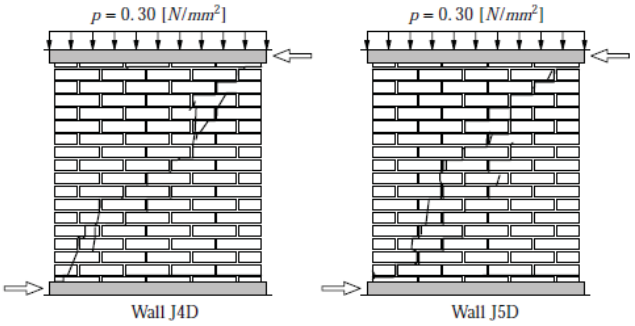

a) Walls without window opening

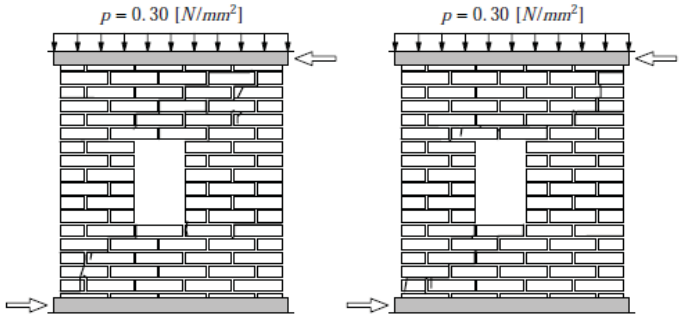

b) Walls with window opening

Figure 4.5. Experimental crack patterns for different masonry walls analyzed by Lourenço [1996].

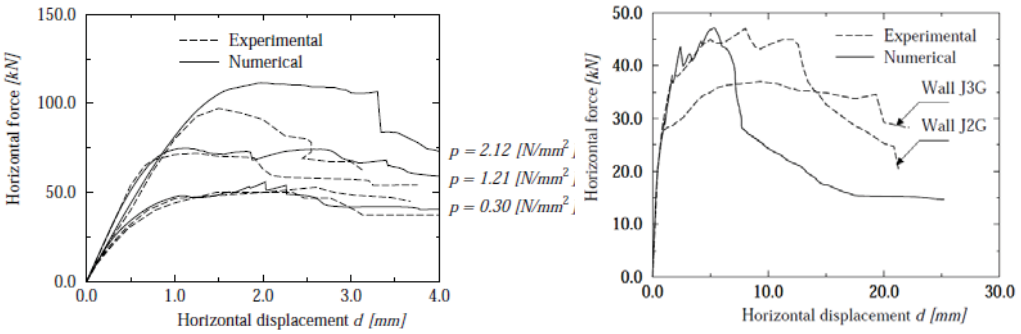

a) Pushover of walls without opening **b) Pushover curves of walls with opening**

Figure 4.6. Comparison of experimental and analytical pushover curves [Lourenço 1996].

From the numerical results it was seen that the central opening defined two small relative piers and forces the compressive strut to spread around both sides of the opening. The pushover curves of the two types of walls are shown in Figure 4.6, where it is seen that there is a reasonable approximation between the numerical models with the experimental results obtained by Raijmakers and Vermeltfoort (1992). According to Lourenço [1996], more continuous stress distribution can be found when increasing initial vertical pre-compression since the opening size of the diagonal cracks are reduced. Besides, Figure 4.6 shows that masonry behaves in a ductile manner, which means that masonry can withstand post-peak deformations with reduced of strength.

Macro-modelling is commonly used for analysis of large structures due to its lower calculation demands. Unlike micro-modelling, it does not make any distinction between bricks and mortar joints, the damage is smeared into the continuum. The input material properties are established by homogenization, which relates average masonry strains and average masonry stresses [Roca *et al.* 2010]. The homogenization involves the simplification of the composite brick-mortar into one equivalent material; this means the creation of a new material which represents the behaviour of the masonry. The homogenization can be computed in one direction first (either parallel or perpendicular to the bed joints) and then in the other direction [Sui and Rafiq 2009].

Macro-models are applicable when the structure is composed of solid walls with sufficiently large dimensions so that the stresses across or along a macro-length areessentially uniform [Lourenço 1996]. This technique has been used for analysis of arch bridges, historical buildings, mosques and cathedrals, Figure 4.7 [Roca *et al.* 2010], based on tension-compression damage finite element formulation. Within a finite element approach, the micro-modelling can be represented by a discrete approach and the macro-modelling by a continuum approach; both based on cracking or damaged models.

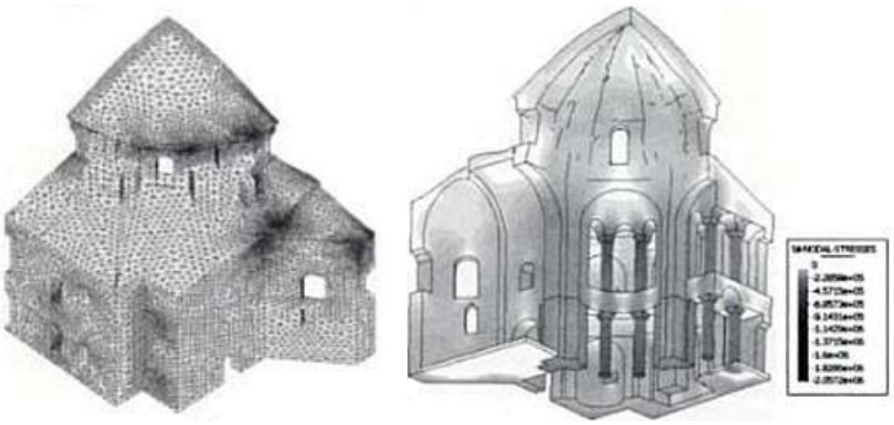

a) Finite element model **b) Distribution of stresses due to gravity loads**

Figure 4.7. Analysis of Kuçuk Ayasofya Mosque (Istanbul) by Roca *et al.* [2010] following a macro modelling approach.

4.2 FINITE ELEMENT APPROACHES FOR MASONRY MODELLING

The masonry material can be modelled following fracture mechanics or continuum mechanics. The first, known as discrete approach, assumes damage at specific zones (which can be the mortar joints, Figure 4.8a), while the second predicts cracking and damage all over the continuum (Figure 4.8b). The failure assessment of concrete structures is mainly dependent on the proper modelling of the constitutive behaviour [Feenstra and de Borst 1992; Feenstra and Rots 2001]. Masonry, as well as concrete, resists compression relatively well, but can only resist low tensile stresses with a fast reduction of the stress in the plastic zone (tension-softening).

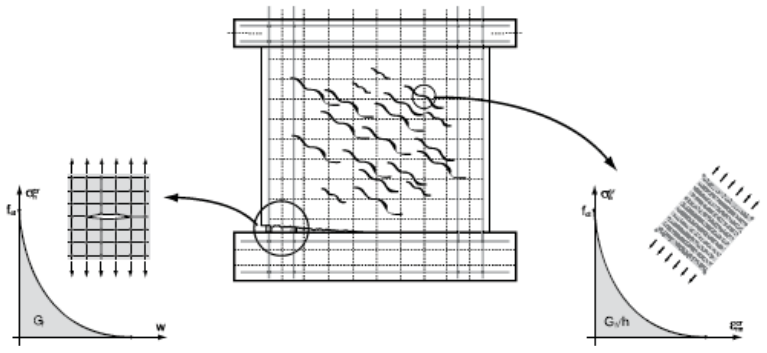

a) Discrete crack model **b) Smeared crack model**

Figure 4.8. Concrete crack models [Midas FEA v2.9.6 2009].

4.2.1 Fracture mechanics approach: discrete model (micro-modelling)

The discrete model initially introduced by Ngo and Scordelis [1967] for modelling concrete, assumes discontinuos elements interacting with material cracks represented as boundaries with zero thickness. If the failure mechanism is known and the crack path can be identified, the discrete crack model represents the fracture most accurately. For example, if it is known that the crack path on a masonry panel follows the head and bed joints, these joints can be modelled as discontinuous.

The simplified micro-modelling of masonry is part of the discrete concept, where the inelasticity is mainly concentrated at the brick-mortar interface. The bricks can be modelled as elastic or even as inelastic. Lourenço [1994] developed a composite interface plasticity based model for masonry capable of representing the typical interface failure modes, such as cracking of the joints, sliding along the bed or head joints at low values of normal stress, and crushing at bricks and mortar joints (see Section 5.2).

The main input data for this model are the constitutive laws for representing the tension, shear and compression behaviour of the mortar joints (Figure 4.9). In these laws the inelastic part is represented by the fracture energy, which is the area under the stress-displacement curve at the softening part. This composite interface model is developed under plasticity concepts and allows the physical separation of bricks and mortar joints.

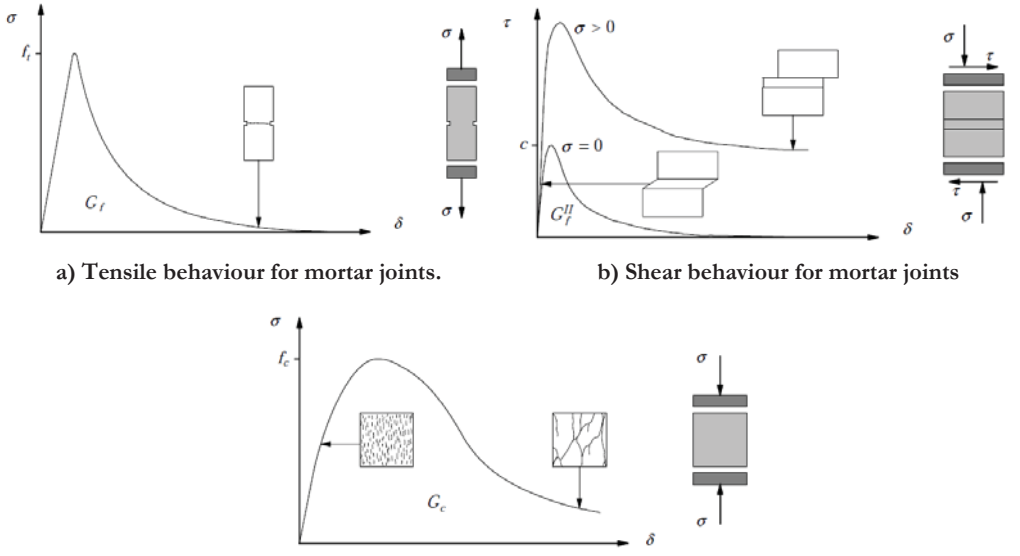

a) Tensile behaviour for mortar joints. **b) Shear behaviour for mortar joints**

c) Compressive behaviour of bricks and mortar joints

Figure 4.9. Stress-displacement diagrams for quasi brittle materials [Lourenço 1996].

4.2.2 Continuum mechanics approach: plasticity and damage mechanics (macro modelling)

Generally, continuum models can be represented by smeared crack models and by damaged plasticity models.

The smeared crack model uses continuum elements where the concrete/masonry cracks are assumed smeared and distributed all over the model in terms of strain [Midas FEA v2.9.6 2009]. The fracture process is initiated when the maximum principal stress in a material point exceeds its tensile strength. The crack propagation is mainly controlled by the shape of the tensile-softening diagram and the material fracture energy, which is normalized by a characteristic element length *h* [Cruz *et al.* 2004]. The tension and compression constitutive law are the principal input data for this model (Figure 4.10).

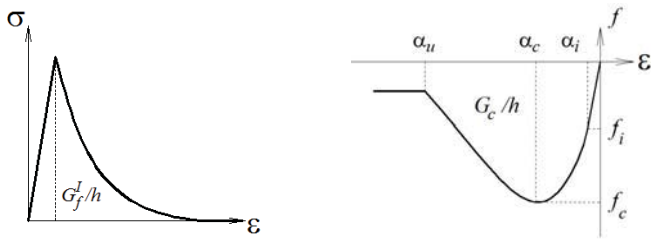

a) Tensile behaviour **b) Compression behaviour**

Figure 4.10. Constitutive law for masonry composite (stress-strain curves).

The smeared crack model can follow a decomposed-strain model or a total strain model, in either fixed or rotated axes. The former allows decomposing the total strain as the sum of the material strain plus the crack strain. The material strain can include the elastic strain, creep strain, thermal strain, etc. According to Rots [2002] it has been proven to be effective to decompose the strain into a part that belongs to the crack and a part that belongs to the material at either side of the cracks. The crack strain of the decomsposed-strain model can be addressed with the theory of plasticity [Feenstra 1993], where the important characteristic is the existence of a yield function that bounds the elastic domain.

The total strain model does not divide the total strain into strain components, making the analysis easier and faster. The material properties make uses only of the constitutive law for tension and compression (stress-strain relationships). Similarly to the previous model, the fracture energy over the characteristic element leght (G_f/h) is represented by the area under the inelastic part of the stress-strain curves. The advantage of using this model is

the easy formulation of the algorithm, since it only uses stress-strain relationships and may be easier to understand by users.

The smeared crack model can be further classified into single-fixed (Figure 4.11a), multiple fixed and rotated crack formulations (Figure 4.11b). The first one, known as orthogonal model, assumes orthogonal crack directions, which means that the direction of new cracks coincides with the maximum principal stress orientation at crack initiation. In a plane stress state, only two crack directions can form and remain fixed throughout the loading process. However, the principal stresses can change their orientation and can exceed the tensile strength, leading to a numerical response stiffer than the experimental observations [Ohmenhauser *et al.* 1998].

The multiple fixed crack model is similar to the orthogonal model, the only difference being that the crack orientation is updated in a stepwise manner allowing secondary cracks to develop if a predefined threshold angle is exceeded.

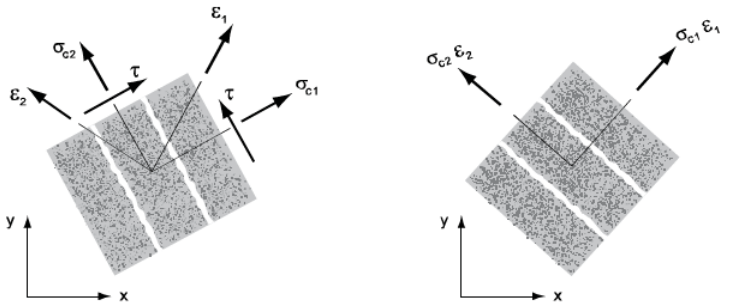

a) Fixed crack model **b) Rotating crack model**

Figure 4.11. Orthogonal crack models [Midas FEA v2.9.6 2009].

In the non-orthogonal model, introduces by Cope *et al.* [1980], the crack direction can rotate and, once more, exceed the tensile strength [Elsaigh 2007]. The local crack coordinate system is continuously rotating with the modification of the direction principal axe.

In the damage plasticity model the two main failure mechanisms are tensile cracking and compressive crushing of the material. Similar to the smeared crack model, the damage of the material is smeared into the continuum. This model assumes that material failure can be effectively modelled using its uniaxial tension, uniaxial compression and plasticity characteristics. The cracking in the concrete model is represented by the damage factors that reduce the elasticity modulus in tension and compression. A detail explanation of this model is given in section 5.5.

4.3 EXAMPLES OF NUMERICAL MODELLING ON MASONRY PANELS

Lotfi and Shing [1994] followed a simplified micro-modelling for simulating the in-plane failure of unreinforced masonry walls. Since the fracture of the mortar joints usually dominates the behaviour of unreinforced masonry structures subjected to seismic loadings, proper modelling of the behaviour of these joints was addressed by a dilatancy interface constitutive model. The bricks were modelled following a smeared crack approach, which assumes that locally generated cracks are evenly spread over a wide surface.

The constitutive model for the mortar joints was developed in terms of plasticity, by using non-associated flow rule, which is used for better characterization of masonry [Lourenço 1996]. The performance of this dilatant interface constitutive model was compared with the experimental results obtained from Amadei *et al.* [1989] showing that the numerical model is not only capable of predicting the load-carrying capacity of a masonry assemblage, but it also provides detailed information on the failure mode, ductility, and crack patterns (Figure 4.12a). Experimental results indicate that for a given compressive stress, the rate of dilatancy decreases with increasing cumulative relative tangential displacements [Lotfi and Shing 1994; Lourenço 1996; Pande *et al.* 1990]. Figure 4.12b shows the pushover curve of the experimental curve and the numerical results.

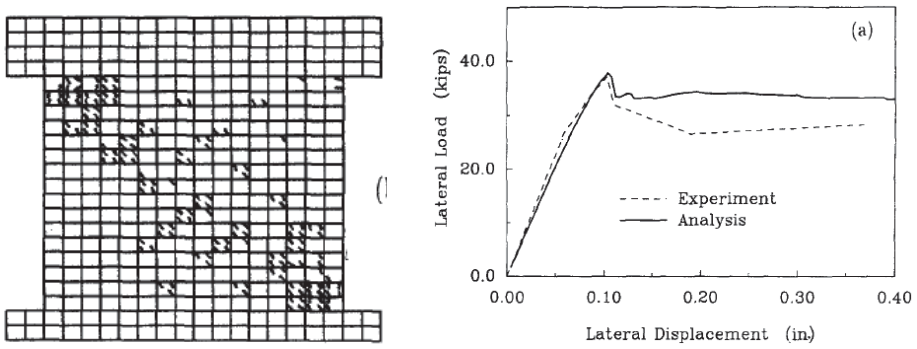

a) Final crack pattern in masonry units **b) Comparison of pushover curves**

Figure 4.12. Analysis of numerical results of an unreinforced masonry wall made by Lotfi and Shing [1994].

Stavridis and Shing [2010] modelled the non linear behaviour of masonry-infilled RC frames based on the smeared crack model (for bricks) and interface models (for mortar joints) developed by Lotfi and Shing [1994], again following a simplified micro-modelling. The models were implemented in the finite element program FEAP [Taylor 2007] and the results were compared with those from experimental tests carried out by Mehrabi *et al.* [1994]. The infill bricks were modelled by two rectangular continuum elements that are

inter-connected through a vertical interface element, as seen in Figure 4.13. This allows modelling the tensile splitting of the brick units and the relative sliding motion in fractured unit. The joints were modelled with a zero-thickness cohesive interface model.

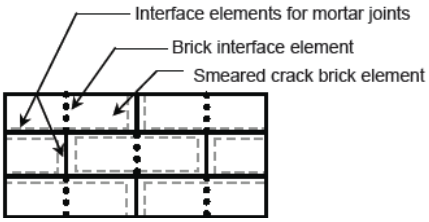

Figure 4.13. Finite element discretization of masonry infill [Stavridis and Shing 2010]**.**

The smeared crack model uses plasticity concepts for simulating the compressive failure and a simple non linear orthotropic material law for simulating the tensile fracture process of bricks. Figure 4.14 shows the comparison between the load-displacement relations obtained from the finite element models and from the experimental tests.

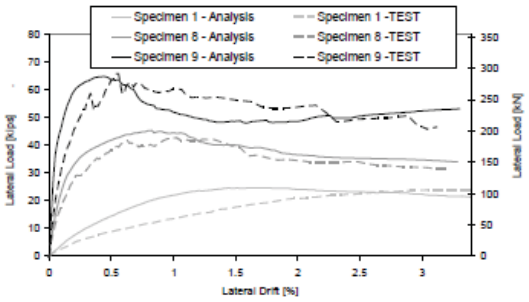

Figure 4.14. Comparison of pushover curves analyzed by Stavridis and Shing [2010].

The strength and post-peak behaviour of the numerical models match the experimental results well. The proposed modelling scheme is able to capture the different failure mechanisms (Figure 4.15), where the failure initiated with the formation of a stair-stepped diagonal/sliding crack in the infill that was followed by a distinct diagonal shear crack at the top of the column. As the lateral drift increases, the damage is governed by severe slips along a large number of bed joints in the infill. Stavridis and Shing [2010] conclude that the mortar joint properties are the most influential parameters in the response of the numerical model.

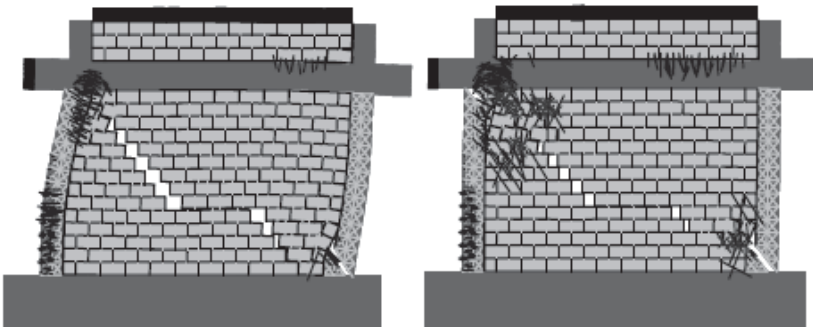

Figure 4.15. Numerical failure pattern of the masonry infill wall analyzed by Stavridis and Shing [2010].

Attard *et al.* [2007] developed another finite element procedure, which is based on the simplified micro-modelling concept, for the simulation of the tensile and shear fracture in masonry as an extension of the work presented by Attard and Tin-Loi [1999, 2005]. The numerical implementation allows to model the mortar joints, which represents a plane of weakness, as an interface of zero thickness or of given thickness. In this case, the fracture is captured through a constitutive softening-fracture law at the interface nodes boundaries. The inelastic failure properties are divided into those for the mortar joints and those for fracture within the unit bricks. The inelastic failure surface is modelled using a Mohr–Coulomb failure surface with a tension cut-off without compression cap (Figure 4.16), so no compression failure is modelled. The basic unit in the formulation is a triangle which two nodes on each of the three side/interfaces (Figure 4.17). Masonry is modelled by combining the triangle units to form a brick with the interfaces around the brick representing the mortar interface.

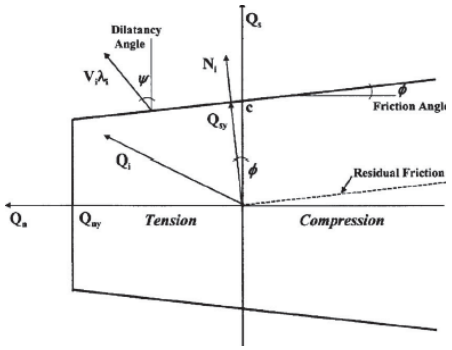

Figure 4.16. Mohr Coulomb with tension cut-off inelastic failure surface [Attard *et al.* 2007].

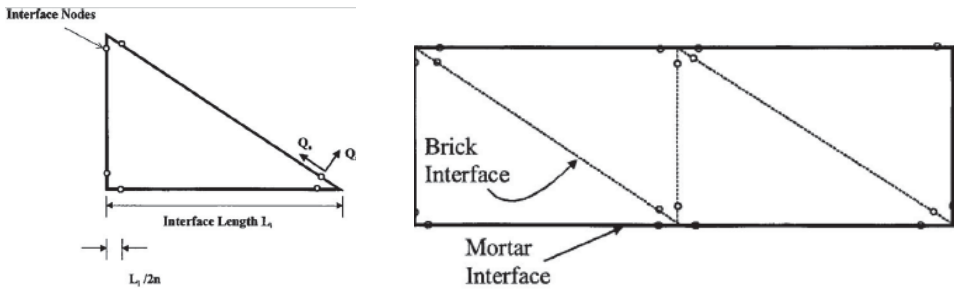

a) Basic triangular unit **b) Single masonry unit**

Figure 4.17. Modelling of masonry units by Attard *et al.* [2007].

Three numerical models were used to demonstrate the applicability of the finite element procedure. The first model deals with tension parallel to a bed joint but involves both tension cracking and cohesion/shear degradation. The results were compared with the ones given by Lourenço [1996] and Lourenço *et al.* [1999], where continuum elements were used for the brick units and interface elements for the mortar joints. The second numerical model was able to represent the shear behaviour under different confining pressures; the results were compared with the experimental data provided by Van Der Pluijm [1993]. The last numerical model by Attard *et al.* [2007] deals with the bending of a masonry panel with weak and strong mortar. The results were compared with the experiments by Guinea *et al.* [2000]. It seems that the finite element formulation proposed by Attard *et al.* [2007] represents fairly well the masonry behaviour, with emphasis on the tension, sliding and dilatancy phenomena. However, no compression failure is modelled.

Yi [2004] analyzed a variety of elastic and inelastic analytical approaches of a full-scale two-story URM structure tested at the US Construction Engineering Research Laboratory (CERL, Figure 4.18a). The elastic analysis was made by using a three dimensional finite element model with the objective of capturing the initial response of the test. However, this type of analysis is very limited for URM due to the fast excursion into the inelastic range of the masonry. The main result of this elastic model was the evidence of little coupling between parallel in-plane walls; which indicate that two-dimensional analytical approaches can be used to analyze the URM buildings.

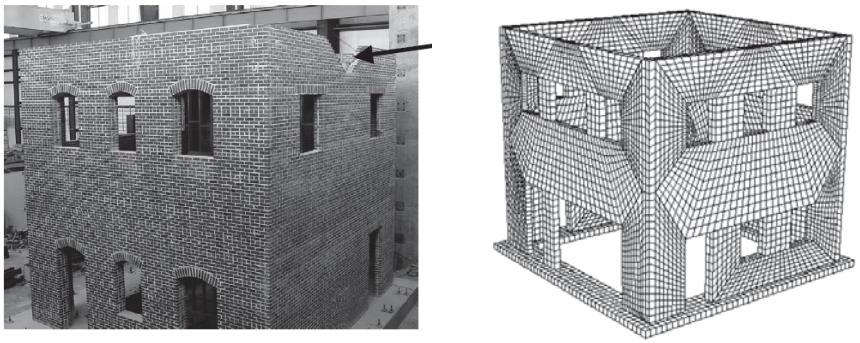

a) Experimental test **b) Abaqus 3D contact model for the test structure**

Figure 4.18. Experimental test and analytical approach of an URM building [Yi 2004].

A 3D nonlinear finite element model and 2D nonlinear pushover analysis were used to analyze the nonlinear response of the tested URM building. The 3D nonlinear finite element model was a combination of rigid blocks interacting between them through contact surfaces (Figure 4.18b), trying to represent the wall overturning. This FE model was not intended to address every possible crack at the interface between bricks and mortar, so potential macro cracks were previously identified and placed as contact surfaces. The element uses a Coulomb friction model to describe the shear capacity of the contact surface.

The numerical model for a URM perforated in-plane wall (2D nonlinear model) is carried out based on assumptions on the relationships between strong spandrel-weak piers (Figure 4.19). This implies that piers crack first, thus averting the failure of spandrels. The model employs several parallel pier springs to simulate the response of each story. The response of the entire wall is determined by combining each story as series springs. The strong spandrel-weak piers model is considered the most accurate model among the available simplified models as 'strong pier-weak spandrel' and 'equivalent frame models' [Yi *et al.* 2006]. The model is then subjected to monotonically increasing lateral forces or displacements until either a target displacement is exceeded or the building collapses.

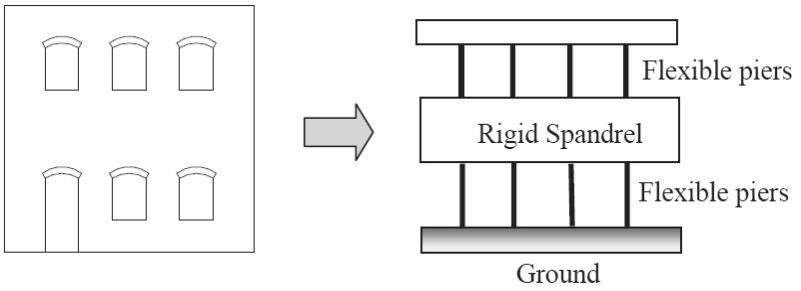

Figure 4.19. Solid spandrel-cracked pier perforated URM wall model [Yi 2004].

Yi *et al.* [2006] conclude that a 3D nonlinear finite element analysis is good for deep investigation but time consuming and sometimes unstable due to convergence problems. They also concluded that the 2D nonlinear pushover method is best for seismic evaluation and retrofit of existing URM structures, although it is based on the strong spandrel-weak pier assumption.

4.4 SUMMARY

The analysis of failure of masonry structures is usually based on modelling approaches applied to concrete mechanics (*e.g.* fracture mechanics). A masonry structure can be modelled following a micro-modelling or a macro-modelling technique within the finite element method. The first one represents the elastic and inelastic behaviour of the mortar joints and of the bricks. Usually, the inelastic phenomena are placed at the mortar joints with an interface model that represents the tension and shear behaviour at the joints and the compression failure of the composite brick-mortar. Another way to model a masonry panel is following a macro-modelling technique, where there is not distinction between bricks and mortars and a new material is created taking into account the material properties of the bricks and mortar joints. The cracks are assumed to be over the entire model. This last technique can be applied to adobe structures since there is not a major difference between the adobe brick and the mud mortar joint properties. It can be assumed that adobe masonry behaves as a homogeneous material.

In the micro-modelling case, a finite element model that follows the discrete approach is used. In the case of macro-modelling, the continuum approach is applied. Both finite element models are based on the plasticity theory and will be used in the next sections for modelling adobe structures. Another approach for representing the behaviour of masonry is by the equivalent frame method, which is based on strongly simplifying hypotheses on the geometry and the mechanical behaviour of the masonry structure [*e.g.* Calderini *et al.* 2009; Magenes and Della Fontana 1998]; however, this approach is not following here.

5. DISCRETE AND CONTINUUM MODELS FOR REPRESENTING THE SEISMIC BEHAVIOUR OF MASONRY

The material behaviour of a model (body) can be reproduced through a Finite Element idealization making use of stress-strain relationships (constitutive models) that represents the stress state in a material point of the body. Specifically for quasi brittle materials, the material cracking can be modelled using two general approaches: discrete and continuum. These approaches have been studied by many authors [*e.g.* Lotfi and Shing 1994; Ngo and Scordelis 1967; Rots 1991] and also applied to masonry structures. This chapter describes the concepts of each approach and its mathematical formulation, with details on the application to masonry structures.

5.1 REVIEW OF THEORY OF PLASTICITY

Plasticity is a tool for describing ductile material behaviours. Plasticity describes materials, such as ductile metals, clay or putty, which allows bodies to change their shape by the application of forces, and retain their new shape upon removal of such forces [Lubliner 2006]. This means that materials exhibit permanent or irreversible deformations also after unloading. Tipically plastic materials are metals, but plasticity is extended to brittle materials because of its computational advantages. Materials such as soils, rock and concrete, can be defined as plastic materials with great sensitivity to pressure, resulting in very different strengths in tension and compression.

The important characteristic in the plasticity theory is the existence of a yield function that bounds the elastic domain. The essential elements of any constitutive model based on the classical plasticity theory are the yield criterion, which determine if the material responds purely elastically at a particular state of stress; the flow rule, which defines the inelastic deformation that occurs if the material point is no longer responding elastically; and the hardening rule, which defines the way in which the yield and flow rule change as inelastic deformation occurs [Koiter 1960].

In problems where tension plays a significant role, the usual procedure is to apply plasticity theory at the compression zone and treat zones in which at least one principal stress is tensile by fracture mechanics [Lubliner *et al.* 1989; Malm 2009].

5.1.1 Fundamentals

The incremental theory of plasticity allows decomposing the strain rate $\dot{\varepsilon}$ as the sum of elastic strain rate $\dot{\varepsilon}^{el}$ and a plastic strain rate $\dot{\varepsilon}^{pl}$, which represent the reversible and irreversible strains, respectively:

$$\dot{\varepsilon} = \dot{\varepsilon}^{el} + \dot{\varepsilon}^{pl} \tag{5.1}$$

The stress rate can be expressed as a function of the elastic stiffness matrix $\boldsymbol{D}$ and the elastic strain rate $\dot{\varepsilon}^{el}$:

$$\dot{\boldsymbol{\sigma}} = \boldsymbol{D} \cdot \dot{\varepsilon}^{el} = \boldsymbol{D}\left(\dot{\varepsilon} - \dot{\varepsilon}^{pl}\right) \tag{5.2}$$

The principal ingredients for problems involving classical plasticity theory are the yield criterion, the flow rule and the hardening rule.

5.1.2 Yield criterion

A yield criterion or yield surface is a hypothesis defining the limit of elasticity in a material and the onset of plastic deformation under any possible combination of stresses. The state of stress of inside the yield surface is elastic. The yield criterion of a material is defined through experiments on various stress states [Malm 2009]. The stresses at a point can be expressed by a function in the stresses space as follows:

$$f\left(\boldsymbol{\sigma}, k\right) = 0 \tag{5.3}$$

where f is the yield function and k is the hardening parameter variation, which is a measure of the amount of hardening or softening. Yielding can only occur if the stresses $\boldsymbol{\sigma}$ satisfy the previous equation: if f is less or equal than zero, plastic flow does not occur. If f is greater than zero, plastic flow takes place (Figure 5.1).

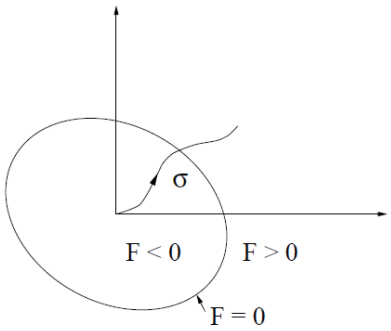

Figure 5.1. Representation of a general yield surface (modified from Saouma [2000]).

Several different yield criteria have been developed for different materials, as seen in Figure 5.2. The Von Mises and Tresca yield criteria was developed for ductile elements as steel; whereas for quasi-brittle materials, the Drucker-Prager and Mohr-Coulomb yield criteria are more appropriated [Malm 2009]. More refined yield criteria have been proposed by [Lubliner *et al.* 1989], where a combination of the Mohr-Coulomb and the Drucker-Praguer yield functions is discussed.

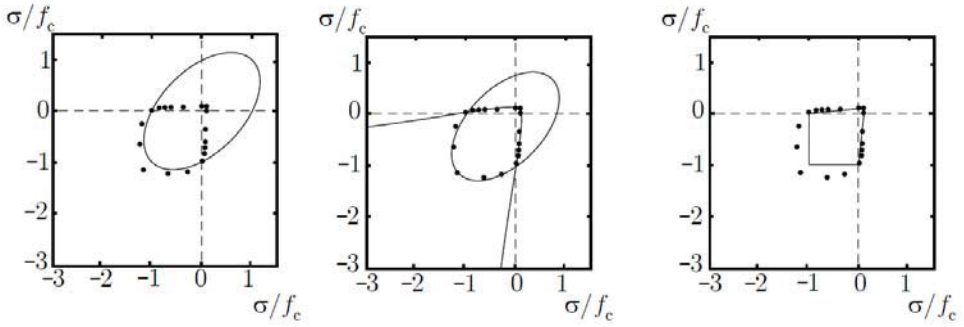

a) Von Mises **b) Drucker-Prager** **c) Mohr-Coulomb**

Figure 5.2. Failure criteria for biaxial stress state illustrated for plane stress state (Modified from Jirasek and Bažant [2002]).

When more than one function is used for characterizing a material behaviour, the elastic domain is defined by a number of functions $f < 0$ and they must satisfy the Kuhn-Tucker conditions: $f \leq 0$, $\dot{\lambda}_i \geq 0$, $\dot{\lambda}_i \cdot f = 0$.

In this case when the yield function f is less or equal than zero, so $\dot{\lambda}_i$ (plastic multiplier rate, see section 5.1.3 for the definition) becomes zero and plastic flow does not occur,

which means the material is in the elastic range. The yield function depends on the variation of plastic strain ε_p.

5.1.3 Flow rule

The flow rule is the necessary kinematic assumption given for plastic deformation or plastic flow. It defines the relative magnitudes of the components of the plastic strain increment tensor $\dot{\varepsilon}^{pl}$. The flow rule also defines the direction of the plastic strain increment vector $\dot{\varepsilon}^{pl}$ in the strain space (Figure 5.3, [Chen and Han 1988]).

The evolution of the inelastic displacement in the fracture process is defined through flow rule. According to Koiter's rule, the flow rule is expressed by scalar and vector components.

$$\dot{\varepsilon}^{pl} = \sum_{i=1}^{n} \dot{\lambda}_i \frac{\partial g_i}{\partial \boldsymbol{\sigma}} = \sum_{i=1}^{n} \dot{\lambda}_i \boldsymbol{m}_i \tag{5.4}$$

where $\dot{\lambda}_i$ is a positive plastic multiplier (which is nonzero only when plastic deformations occur), g_i is the plastic potential function given as a function of the stress tensor $\boldsymbol{\sigma}$ and the hardening parameter k, $\boldsymbol{m}_i$ is a vector defining the direction of plastic strain.

The plastic potential function g_i describes the plastic potential surfaces in stress space and can be expressed as separate variables by:

$$g_i\left(\boldsymbol{\sigma}, \dot{k}\right) = \Phi\left(\boldsymbol{\sigma}\right) + \Omega\left(k\right) \tag{5.5}$$

where Φ and Ω represent generic functions.

The flow rule can be defined as an associated or non associated flow rule. An associated flow rule is such that the direction of the plastic strain $\dot{\varepsilon}^{pl}$ (flow rule) is expressed as $\partial f / \partial \boldsymbol{\sigma}$ rather than using the plastic potential function g_i, so the plastic flow is connected or associated with the yield criterion. This means that the plastic flow develops along the normal to the yield surface (Figure 5.3a). A non-associated flow rule is such that the direction of the plastic strain is defined as $\partial g_i / \partial \boldsymbol{\sigma}$ with $g_i \neq f$; in this case the plastic strain is not directed along the plastic surface (Figure 5.3b).

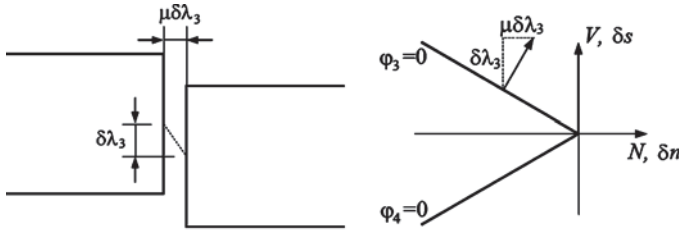

a) Associated flow rule with fix dilatancy (normal separation between blocks)

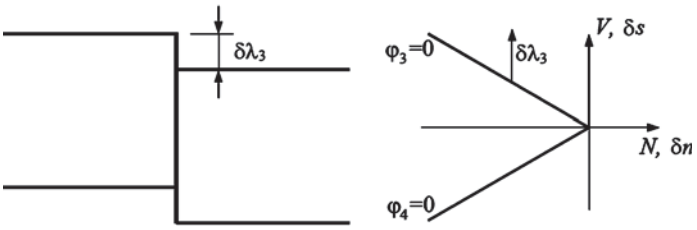

b) Non-associated flow rule with null dilatancy

Figure 5.3. Representation of associated and non-associated flow rule [Roca *et al.* 2010].

For ductile material that follow laws such as von Mises and Tresca, which show constant deviatoric stresses along the hydrostatic pressure in the stress space, an associated flow rule can be used. For brittle materials that follow laws such as Mohr-Coulomb and Drucker-Praguer, which show deviatoric stresses varying with the hydrostatic pressure in the space of stresses, the non-associated flow rule can be used [Midas FEA v2.9.6 2009].

5.1.4 Hardening/softening behaviour

The phenomenon whereby the yield stresses increase, or decrease (hardening or softening), with further plastic straining is called work hardening or strain hardening [Chen and Han 1988]. The yield surface is not fixed in the stress space and its motion, change of size and shape are controlled by the hardening rule.

The variation of the hardening parameter, the scalar $\dot{k}$, is generally related to the equivalent plastic strain rate $\dot{\tilde{\varepsilon}}^{pl}$ (strain hardening) or with the plastic work rate $\dot{W}^{p}$ (work hardening). From the former assumption, the equivalent plastic strain rate defined as:

$$\dot{k} = \dot{\tilde{\varepsilon}}^{pl} = c\sqrt{\left(\dot{\varepsilon}^{pl}\right)^{T} \dot{\varepsilon}^{pl}} \tag{5.6}$$

where c is a coefficient that permits that plastic strain in the loading direction of a uniaxial test be equal to the equivalent plastic strain rate $\dot{\tilde{\varepsilon}}^{pl}$. Usually $c = \sqrt{2/3}$.

The equivalent plastic strain rate can also be derived from the plastic work per unit volume as:

$$\dot{k} = \dot{\bar{\varepsilon}}^{pl} = \frac{\dot{W}^{p}}{\bar{\sigma}} = \frac{\boldsymbol{\sigma}^{T}\dot{\boldsymbol{\varepsilon}}^{pl}}{\bar{\sigma}} \tag{5.7}$$

where $\bar{\sigma}$ is the uniaxial yield stress [Cruz *et al.* 2004].

If the assumption of work hardening is taken into consideration, the rate variable $\dot{k}$ is given by:

$$\dot{k} = \dot{W}^{p} = \boldsymbol{\sigma}^{T}\dot{\boldsymbol{\varepsilon}}^{pl} \tag{5.8}$$

Depending on the hardening behaviour of the materials, three main phenomenological hardening models are usually proposed to represent hardening: isotropic hardening [Odqvist 1933], kinematic hardening [Prager 1955, 1956] and mixed hardening [Hodge 1957]. The first one exhibits the behaviour of isotropic expansion or contraction of the yield surface (Figure 5.4a). The second one exhibits the behaviour of translation of the origin of the yield surface without any expansion or contraction (Figure 5.4b). The third one exhibits the combined behaviour of the two previous phenomenological hardenings (Figure 5.4c).

According to Oliveira [2003], the isotropic hardening law is the easiest one and good results can be achieved under monotonic loading conditions. However, the description of induced anisotropy or other features related to cyclic behaviour, *e.g.* the Bauschinger effect, cannot be suitably described by such a law and therefore more complex hardening laws are required..

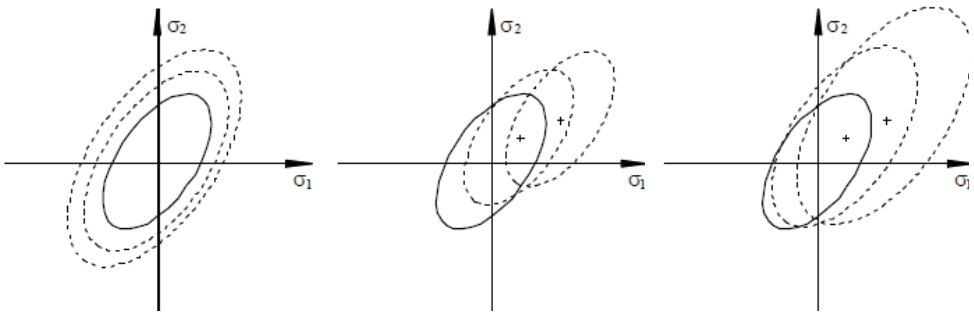

a) Isotropic hardening **b) Kinematic hardening** **c) Mixed hardening**

Figure 5.4. Movement of the yield surfaces. σ_1 and σ_2 are the principal stresses (modified from Cruz *et al.* [2004]).

As follows the finite element approaches, discrete and continuum, for masonry modelling are described in detail. For the first, the composite cracking-shearing-crashing model specified in section 4.2.1 is explained. For the second, the smeared crack model and the damaged plasticity model specified in section 4.2.2 are explained.

5.2 DISCRETE MODEL: COMPOSITE CRACKING-SHEARING-CRASHING MODEL

Interface elements allow discontinuities between two parts of the model and their behaviour is represented in terms of a relation between tractions $\boldsymbol{t}$ and relative displacements $\Delta\boldsymbol{u}$ across the interface through the following equation:

$$\boldsymbol{t} = \boldsymbol{D} \cdot \Delta\boldsymbol{u} \tag{5.9}$$

For 2D formulation (Figure 5.5) the matrices are expressed as:

$$\boldsymbol{t} = \begin{Bmatrix} t_n \\ t_s \end{Bmatrix},\ \boldsymbol{D} = \begin{bmatrix} k_n & 0 \\ 0 & k_s \end{bmatrix},\ \Delta\boldsymbol{u} = \begin{Bmatrix} \Delta u_n \\ \Delta u_s \end{Bmatrix} \tag{5.10}$$

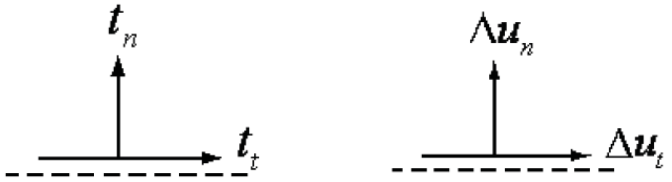

a) Relative traction **b) Relative displacement**

Figure 5.5. Normal and tangential relative traction and displacement in 2D.

And for 3d formulations (Figure 5.6) the matrices are given by:

$$\boldsymbol{t} = \begin{Bmatrix} t_n \\ t_s \\ t_t \end{Bmatrix},\ \boldsymbol{D} = \begin{bmatrix} k_n & 0 & 0 \\ 0 & k_s & 0 \\ 0 & 0 & k_t \end{bmatrix},\ \Delta\boldsymbol{u} = \begin{Bmatrix} \Delta u_n \\ \Delta u_s \\ \Delta u_t \end{Bmatrix} \tag{5.11}$$

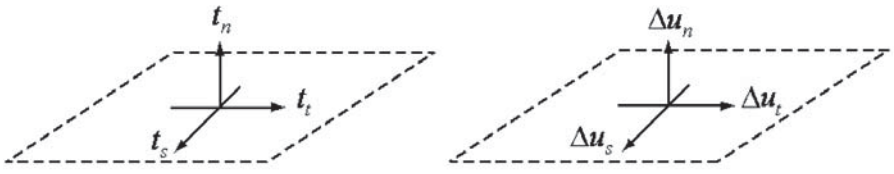

a) Relative traction **b) Relative displacement**

Figure 5.6. Normal and tangential relative traction and displacement in 3D.

The dotted lines represent the interface surface. t_n and Δu_n represent the normal tractions and normal relative displacements, respectively; while t_s and t_t and Δu_s and Δu_t denote the tangential traction and the tangential relative displacement, respectively. The two linear constitutive equations -Equation (5.9)- are uncoupled, *i.e.* the normal traction does not have any influence on the stiffness in the tangential direction.

Since zero thickness is specified for interface elements, the size of the units has to be expanded by the mortar thickness h_m in both directions (Figure 5.7). Penalty stiffness (k_n, k_s, k_t) should be assigned in order not to have numerical problems due to possible interpenetration of blocks. If the penalty stiffness is too low, the interface may yield undesired relative displacements from both sides of the interface element.

Lourenço [1996] suggest computing the penalty stiffness taking into account the contribution of bricks and mortar joints through their elasticity modulus and shear modulus.

$$k_n = \frac{E_u \cdot E_m}{h_m \left(E_u - E_m\right)} \qquad k_s = \frac{G_u \cdot G_m}{h_m \left(G_u - G_m\right)} \tag{5.12}$$

where E_u and E_m are the elasticity modulus and G_u and G_m are the shear modulus for brick and mortar, respectively.

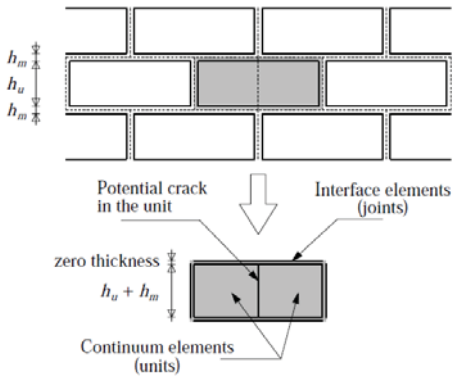

Figure 5.7. Simplified representation of bricks and mortar joints into a numerical model [Lourenço 1996].

The elastic domain is bounded by the interface material model, also known as Composite Interface model in the literature, which simulates fracture, frictional slip as well as crushing along material interfaces, for instance at joints in masonry. Usually the brick units are modelled as linear elastic, or viscoelastic continua, while the mortar joints are

modelled with interface elements, which obey the nonlinear behaviour described by the composite interface model (also known as combined cracking–shearing–crushing model. The law to characterize the inelasticity behaviour is given in terms of plasticity.

Lourenço [1996] used a simplified micro-modelling procedure for analysis of masonry walls, basically for in-plane mechanical behaviour. In this case the inelasticity was concentrated at the interface elements (usually the mortar joints) where crack, slip or crushing can occur. If it is necessary, the inelasticity is also located in the middle of bricks to represent potential pure tensile cracks (Figure 5.7).

This composite interface model is a combination of three plastic surfaces that represent tension, shear and compression failure. A tension cut-off it is considered for tension failure. For the shear failure, the softening process is given by the degradation of the cohesion in Coulomb friction models. For the compression failure, Lourenço [1996] developed a suitable cap model. Each of the failure mechanisms is associated with a hardening/softening rule for representing the inelasticity at any material point. Since the masonry joints have extremely low dilatancy (almost zero, [Lourenço 1996]), the model was formulated in the context of non-associated plasticity.

The principal input data for the composite interface model are the constitutive laws for representing the tension, shear and compression behaviour of the mortar joints. In these laws the inelastic part is represented by the fracture energy, which is the area under the stress-displacement curve at the softening part (inelastic part). The softening is a gradual decrease of the mechanical strength under a continuous increase of deformation. This behaviour is attributed to the heterogeneity of the material, due to the presence of different phases and material defects, such as flaws and voids, and also due to micro-cracks due to shrinkage during curing and the presence of the aggregate [Lourenço 1998].

5.2.1 Two-dimensional interface model

The interface model is derived in terms of generalized stress and strain vectors as follows:

$$\boldsymbol{\sigma} = \begin{pmatrix} \sigma \\ \tau \end{pmatrix}, \qquad \boldsymbol{\varepsilon} = \begin{pmatrix} u \\ v \end{pmatrix} \tag{5.13}$$

where σ and u are the stress and relative displacement in the normal direction of the interface, and τ and ν are the shear stress and relative displacement respectively.

In the elastic range, the constitutive behaviour is described by:

$$\boldsymbol{\sigma} = \boldsymbol{D}\,\boldsymbol{\varepsilon} \tag{5.14}$$

with the stiffness matrix explained before: $\boldsymbol{D} = diag\left[k_n \quad k_s\right]$

5.2.1.1 *Shear-slipping*

The shear-slipping criterion is defined by the following Coulomb friction yield/crack criterion:

$$f = |\tau| + \sigma \cdot \Phi - c \tag{5.15}$$

where τ is the shear stress, Φ is the friction coefficient equal to the friction angle $\tan\phi$, c is the cohesion of the brick-mortar interface. An exponential softening function is assumed for the cohesion. For the friction angle, the softening is taken proportional to the softening of the cohesion. The cohesion softening is defined as follows:

$$c(\sigma, k) = c_0 \exp\left(-\frac{c_0}{G_f^{II}} k\right) \tag{5.16}$$

where c_0 is the initial cohesion of the brick-mortar interface, G_f^{II} is the shear slip fracture energy, k is the hardening parameter.

The friction softening is coupled to the cohesion softening by:

$$\Phi(\sigma, k) = \Phi_0 + (\Phi_r - \Phi_0)\frac{c_0 - c}{c_0} \tag{5.17}$$

where Φ_0 and Φ_r are the initial and the residual friction coefficients, respectively.

The mode II fracture energy, G_f^{II}, increases under increasing confining pressure as seen in experimental results by Van Der Pluijm [1993]. The experimentally observed linear relation between the fracture energy and the normal confining stress is defined as:

$$G_f^{II} = \begin{cases} a \cdot \sigma + b & if \ \sigma < 0 \\ b & if \ \sigma \geq 0 \end{cases} \tag{5.18}$$

Where a and b are constants determined by linear regression of the experimental data.

Dilatancy

The non-associated flow rule is expressed as follows:

$$\dot{\boldsymbol{\varepsilon}}_{\boldsymbol{p}} = \begin{Bmatrix} \dot{u}_p \\ \dot{v}_p \end{Bmatrix} = \dot{\lambda} \frac{\partial g}{\partial \boldsymbol{\sigma}} \tag{5.19}$$

The plastic potential function for describing the dilatancy is given by:

$$\frac{\partial g}{\partial \boldsymbol{\sigma}} = \begin{Bmatrix} \Psi \\ sign(\tau) \end{Bmatrix} \tag{5.20}$$

where $\Psi = \tan\psi$ is the mobilized dilatancy coefficient. From Equations (5.19) and (5.20) the following equation is obtained:

$$\psi = \frac{\dot{u}_p}{\dot{v}_p} sign(\tau) \tag{5.21}$$

By integration, the shear-slip induced normal uplift is found to be:

$$u_p = \int \Psi \, d\left|\Delta v_p\right| \tag{5.22}$$

The dilatancy is considered as a function of the plastic relative shear displacement and the normal confining pressure. Under increasing value of these two quantities, the dilatancy angle tends to zero. The dilatancy formulation, Equation(5.23), can be expressed as separate values to simplify curve fitting and to ensure convexity of the potential function *g*:

$$\Psi = \Psi_1(\sigma)\Psi_2(v_p) \tag{5.23}$$

$$g = \int \left(\frac{\partial g}{\partial \sigma}\right)^T d\boldsymbol{\sigma} = |\tau| + \Psi_2(v_p) \int \Psi_1(\sigma) d\sigma \tag{5.24}$$

Therefore, a description of the normal uplift upon shear-slipping is:

$$u_p = \begin{cases} 0 & \text{if } \sigma < \sigma_u \\ \dfrac{\Psi_0}{\delta}\left(1 - \dfrac{\sigma}{\sigma_u}\right)\left(1 - \exp\left(-\delta \cdot v_p\right)\right) & \text{if } \sigma_u \le \sigma < 0 \\ \dfrac{\Psi_0}{\delta}\left(1 - \exp\left(-\delta \cdot v_p\right)\right) & \text{if } \sigma \ge 0 \end{cases} \tag{5.25}$$

which yields after differentiation in

$$\Psi = \begin{cases} 0 & if\ \ \sigma < \sigma_u \\ \Psi_0 \left(1 - \dfrac{\sigma}{\sigma_u}\right) \exp\left(-\delta \cdot v_p\right) & if\ \ \sigma_u \le \sigma < 0 \\ \Psi_0 \exp\left(-\delta \cdot v_p\right) & if\ \ \sigma \ge 0 \end{cases} \tag{5.26}$$

where Ψ_0 is the dilatancy at zero normal confining stress and shear slip. σ_u is the confining stress at which the dilatancy becomes zero. The dilatancy shear slip degradation coefficients δ are material parameters to be obtained from experimental data.

Softening

The strain softening behaviour is controlled by the shear plastic relative displacement (shear-slipping):

$$\dot{k} = \left|\Delta \dot{v}_p\right| = \dot{\lambda} \tag{5.27}$$

According to Midas FEA v2.9.6 [2009], the stress-update can be cast in the standard plasticity predictor-corrector fashion and the corrected stresses, together with the plastic strain increment $\dot{k}$, or $\dot{\lambda}$, can be solved by a Newton-Raphson iterative scheme. A consistent tangent modulus is employed for the global convergence iterations.

With the assumptions given above, reasonable agreement with experimental results was found by Lourenço [1996], (Figure 5.8).

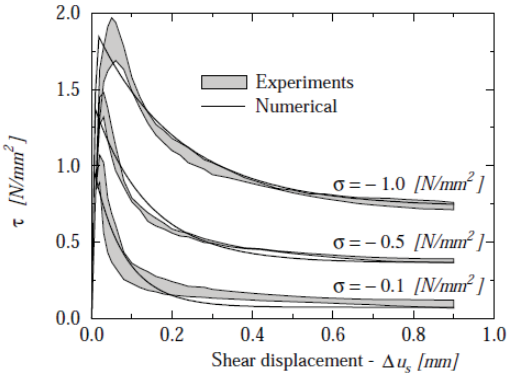

Figure 5.8. Numerical and experimental shear behaviour of mortar joints reported by Lourenço [1996].

5.2.1.2 *Tension cut-off criterion*

The yield function for the tension cut-off is given by:

$$f_2 = \sigma - \sigma_t \tag{5.28}$$

where σ_t is the tensile or brick-mortar bond strength. The strength is assumed to soften exponentially (Figure 5.9) and is governed by:

$$\sigma_t = f_t \exp\left(\frac{f_t}{G_f^I} k_2\right) \tag{5.29}$$

where f_t is the bond strength, G_f^I is the mode I fracture energy, k_2 is the hardening parameter. The softening is governed by a strain softening hypothesis with an associated flow rule, see Equations(5.30) and (5.31), respectively.

$$\dot{k}_2 = \left|\dot{u}_p\right| \tag{5.30}$$

$$\dot{\varepsilon}_p = \dot{\lambda}_2 \frac{\partial f_2}{\partial \boldsymbol{\sigma}} \tag{5.31}$$

Assuming that only the normal plastic relative displacement controls the softening behaviour:

$$\dot{k}_2 = \dot{\lambda}_2 \tag{5.32}$$

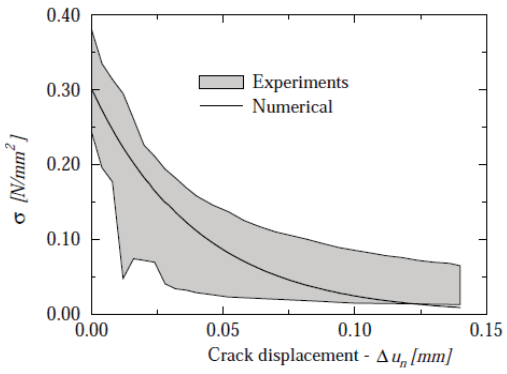

Figure 5.9. Numerical and experimental tensional behaviour of mortar joints reported by Lourenço [1996].

5.2.1.3 *Compression cap*

The yield function for the compression cap is defined as:

$$f_3 = \sigma^2 + C_s \tau^2 - \sigma_c^2 \tag{5.33}$$

C_s is a parameter controlling the shear stress contribution to failure, and σ_c is the compressive strength. The latter is assumed to evolve according to following the strain hardening equation.

$$\dot{k}_3 = \sqrt{\dot{\varepsilon}_p^T \cdot \dot{\varepsilon}_p} \tag{5.34}$$

Upon consideration of an associated flow rule, Equation (5.34) derives in:

$$\dot{\varepsilon}_p = \dot{\lambda}_3 \frac{\partial f_3}{\partial \sigma} \tag{5.35}$$

$$\dot{k}_3 = 2\dot{\lambda}_3 \sqrt{\sigma^2 + \left(C_s \tau\right)^2} \tag{5.36}$$

For the hardening/softening behaviour the law expressed in Equation (5.37) is adopted (see Figure 5.10). The peak strength f_c is reached at the plastic strain k_p. The fracture energy is represented by G_f^c and governs the softening branch. It is recognized that when compressive softening is completed, no further material strength should be available for shear and tension.

$$\begin{aligned}
\bar{\sigma}_1\left(k_3\right) &= \bar{\sigma}_i + \left(f_c - \bar{\sigma}_i\right)\sqrt{\frac{2k_3}{k_p} - \frac{k_3^2}{k_p^2}} \\
\bar{\sigma}_2\left(k_3\right) &= f_c + \left(\bar{\sigma}_m - f_c\right)\left(\frac{k_3 - k_p}{k_m - k_p}\right)^2 \\
\bar{\sigma}_3\left(k_3\right) &= \bar{\sigma}_r + \left(\bar{\sigma}_m - \bar{\sigma}_r\right)\exp\left(2\left(\frac{\bar{\sigma}_m - f_c}{k_m - k_p}\right)\left(\frac{k_3 - k_m}{\bar{\sigma}_m - \bar{\sigma}_r}\right)\right)
\end{aligned} \tag{5.37}$$

where $\bar{\sigma}_i = \frac{1}{3} f_c$, $\bar{\sigma}_m = \frac{1}{2} f_c$ and $\bar{\sigma}_r = \frac{1}{7} f_c$

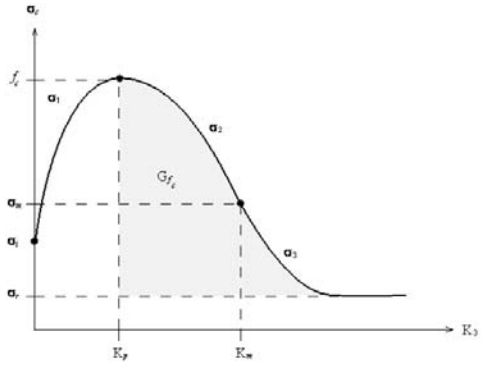

Figure 5.10. Hardening/softening compression law for masonry [Lourenço 1996].

Corners

At each of the intersections of the Coulomb friction criterion with the tension cut-off and the compression cap, the plastic strain increment is given by:

$$\dot{\varepsilon}_p = \dot{\lambda}_1 \frac{\partial g_1}{\partial \sigma} + \dot{\lambda}_i \frac{\partial g_i}{\partial \sigma} \tag{5.38}$$

Subscript 1 refers to shear criterion and *i*, which can be 2 or 3, refers to tension cut-off or compression cap, respectively. In both the shear/tension corner and the shear/compression corner, the stress corrections can be written in a standard predictor-corrector fashion and solved with the two plastic strain increments $\dot{\lambda}_1$ or $\dot{\lambda}_i$ with a Newton-Raphson scheme [Lourenço 1996].

5.2.2 Three-dimensional interface model

The 3D yield function, without considering the compression cap model, is shown in Figure 5.11 [Midas FEA v2.9.6 2009]. The generalized stress and strain vectors are shown in the following equation:

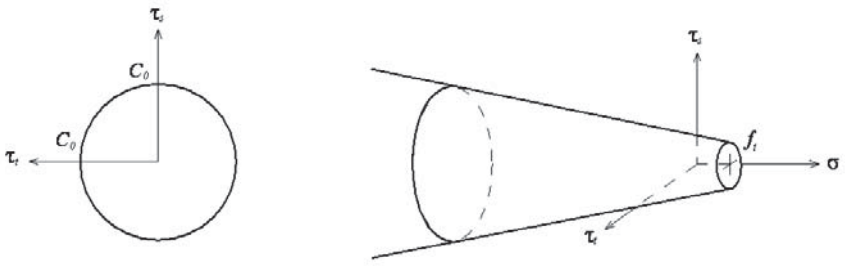

Figure 5.11. Three-dimensional interface yield function (modified from Midas FEA v2.9.6 [2009]).

$$\boldsymbol{\sigma} = \begin{pmatrix} \sigma \\ \tau_s \\ \tau_t \end{pmatrix}, \qquad \boldsymbol{\varepsilon} = \begin{pmatrix} u \\ v \\ w \end{pmatrix} \tag{5.39}$$

where σ and ε are the stress and relative displacement normal to the plane, τ_s and τ_t are the shear stresses acting in the local interface plane, and v and w are the relative shearing displacements in the interface plane.

In the elastic regime, the constitutive behaviour is described by:

$$\boldsymbol{\sigma} = \boldsymbol{D}\boldsymbol{\varepsilon} \tag{5.40}$$

With the stiffness matrix $\boldsymbol{D} = diag\left[k_n \quad k_s \quad k_t\right]$.

For the tension cut-off, the yield function remains the same as the one expressed in Equation (5.29). For the shear-slipping the Coulomb friction yield function is expressed by:

$$f = \sqrt{\tau_s^2 + \tau_t^2} + \sigma \cdot \Phi - c \tag{5.41}$$

The cohesion and friction softening are expressed by Equations (5.16) and (5.17), respectively. A non-associated plastic potential is chosen giving the following flow rule:

$$\dot{\varepsilon}_p = \dot{\lambda}\frac{\partial g}{\partial \boldsymbol{\sigma}} = \dot{\lambda}\left[\psi \quad \frac{\tau_s}{\sqrt{\tau_s^2 + \tau_t^2}} \quad \frac{\tau_t}{\sqrt{\tau_s^2 + \tau_t^2}}\right]^T \tag{5.42}$$

The mobilised dilatancy Ψ is defined in Equation (5.26). The strain softening (hardening parameter) is governed by the equivalent shear displacement:

$$\dot{k} = \sqrt{\left(\dot{v}_p\right)^2 + \left(\dot{w}_p\right)^2} = \dot{\lambda} \tag{5.43}$$

5.3 SMEARED CRACK MODEL: DECOMPOSED-STRAIN MODEL

The decomposed-strain model calculates the total strain in terms of elastic, plastic and crack strain. Based on the work presented by Cruz *et al.* [2004] the decomposed smeared crack model is explained as follows for tension behaviour, where the plastic strain is almost neglected.

The orthogonal smeared crack model is limited by crack directions. In a plane stress state, the first crack is orientated perpendicular to the principal stress axis, and the second cracks are perpendicular to the previous ones. In a 3D modelling, the third crack is perpendicular to the first two cracks.

The total crack strain rate is decomposed into a strain increment vector for the uncracked region between cracks $\Delta\boldsymbol{\varepsilon}^{co}$ and a strain increment vector at the crack $\Delta\boldsymbol{\varepsilon}^{cr}$ as shown in Figure 5.12.

$$\Delta\boldsymbol{\varepsilon} = \Delta\boldsymbol{\varepsilon}^{co} + \Delta\boldsymbol{\varepsilon}^{cr} \tag{5.44}$$

The crack strain increment $\Delta\boldsymbol{\varepsilon}^{cr}$ -Equation (5.45)- represents in a smeared manner the additional deformation due to the opening of cracks at a particular Gauss point.

$$\Delta\boldsymbol{\varepsilon}^{cr} = \sum_{i=1}^{Ncracks} \left(\Delta\boldsymbol{\varepsilon}_i^{cr}\right) \tag{5.45}$$

Figure 5.12. Decomposition of strains [Lotfi and Espandar 2004].

In a crack, two relative displacements define the relative movement of the crack slips: the crack opening displacement w, and a crack sliding displacement s (Figure 5.13). The axes n and t define the local coordinate system of the crack. The crack normal displacement is related to the crack normal strain ε_n^{cr} and the crack sliding displacement to the crack shear strain γ_t^{cr}.

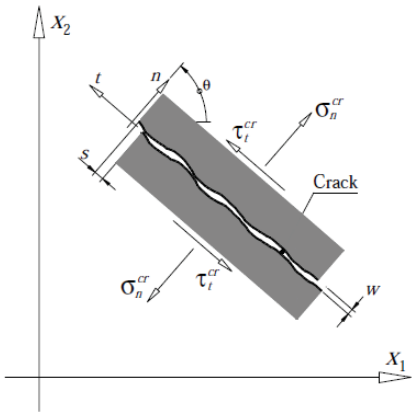

Figure 5.13. Relative displacements and tractions of the crack in the local coordinate system [Cruz *et al.* 2004].

5.3.1 Uncracked state material

A linear elastic stress-strain relationship is adopted for undamaged material. The increment of the total stress $\Delta\boldsymbol{\sigma}$ and strain vectors $\Delta\boldsymbol{\varepsilon}^{co}$ are related as:

$$\Delta\boldsymbol{\sigma} = \boldsymbol{D}^{co}\Delta\boldsymbol{\varepsilon}^{co} \tag{5.46}$$

where $\boldsymbol{D}^{co}$ is the isotropic constitutive matrix of the intact material, see Equation (5.47).

$$\boldsymbol{D}^{co} = \frac{E}{1-\upsilon^2}\begin{bmatrix} 1 & \upsilon & 0 \\ \upsilon & 1 & 0 \\ 0 & 0 & (1-\upsilon)/2 \end{bmatrix} \tag{5.47}$$

where E is the Young's modulus and υ the Poisson's ratio.

5.3.2 Cracked state material

Figure 5.13 shows the morphology of a crack in a plane stress case with relative normal and parallel displacements to the crack plane. Axes n and t are defined in the local crack coordinate system. The crack normal strain is represented by ε_n^{cr}, and the shear crack strain by γ_n^{cr}. The incremental local crack strain is given by $\Delta\varepsilon_n^{cr}$ and $\Delta\gamma_t^{cr}$ as follows:

$$\Delta\boldsymbol{\varepsilon}_l^{cr} = \begin{bmatrix} \Delta\varepsilon_n^{cr} & \Delta\gamma_t^{cr} \end{bmatrix}^T \tag{5.48}$$

The transformation between global and local incremental crack strains may be written as:

$$\Delta\boldsymbol{\varepsilon}^{cr} = \left[T^{cr}\right]^{T} \Delta\boldsymbol{\varepsilon}_{l}^{cr} \tag{5.49}$$

or according to Figure 5.13:

$$\begin{bmatrix} \Delta\varepsilon_{1}^{cr} \\ \Delta\varepsilon_{2}^{cr} \\ \Delta\gamma_{12}^{cr} \end{bmatrix} = \begin{bmatrix} \cos^{2}\theta & -\sin\theta\cos\theta \\ \sin^{2}\theta & \sin\theta\cos\theta \\ 2\sin\theta\cos\theta & \cos^{2}\theta - \sin^{2}\theta \end{bmatrix} \begin{bmatrix} \Delta\varepsilon_{n}^{cr} \\ \Delta\gamma_{t}^{cr} \end{bmatrix} \tag{5.50}$$

Similarly to $\Delta\boldsymbol{\varepsilon}_{l}^{cr}$, the incremental local stress vector $\Delta\boldsymbol{\sigma}_{l}^{cr}$ is defined by:

$$\Delta\boldsymbol{\sigma}_{l}^{cr} = \begin{bmatrix} \Delta\sigma_{n}^{cr} & \Delta\tau_{t}^{cr} \end{bmatrix}^{T} \tag{5.51}$$

where $\Delta\sigma_{n}^{cr}$ and $\Delta\tau_{t}^{cr}$ are the normal and shear crack incremental stress, respectively. Using the transformation matrix $\left[T^{cr}\right]$, a relationship between $\Delta\boldsymbol{\sigma}_{l}^{cr}$ and $\Delta\boldsymbol{\sigma}$, which is the incremental stress vector in global coordinates, is:

$$\Delta\boldsymbol{\sigma}_{l}^{cr} = \left[T^{cr}\right]\Delta\boldsymbol{\sigma} \tag{5.52}$$

A tangent matrix relates the incremental stress vector to the equivalent local crack strains, as:

$$\Delta\boldsymbol{\sigma}_{l}^{cr} = \boldsymbol{D}^{cr}\,\Delta\boldsymbol{\varepsilon}_{l}^{cr} \tag{5.53}$$

Combining Equations (5.52) and (5.53), and substituting into Equation (5.49), the following expression is obtained:

$$\Delta\boldsymbol{\varepsilon}^{cr} = \left[\left(\boldsymbol{T}^{cr}\right)^{T}\left(\boldsymbol{D}^{cr}\right)^{-1}\left(\boldsymbol{T}^{cr}\right)\right]\Delta\boldsymbol{\sigma} \tag{5.54}$$

This equation reflects the influence of an incremental crack strain onto the global stress increment vector. Substituting Equation (5.54) into Equation (5.44), the following expression is obtained:

$$\Delta\boldsymbol{\varepsilon} = \Delta\boldsymbol{\varepsilon}^{co} + \sum_{i=1}^{Ncrack}\left[\left(\boldsymbol{T}^{cr}\right)^{T}\left(\boldsymbol{D}^{cr}\right)^{-1}\left(\boldsymbol{T}^{cr}\right)\right]\Delta\boldsymbol{\sigma} \tag{5.55}$$

Re-ordering the previous equation:

$$\Delta\boldsymbol{\sigma} = \left\{ \left(\boldsymbol{D}^{co} \right)^{-1} + \sum_{i=1}^{Ncrack} \left[\left(\boldsymbol{T}^{cr} \right)^{T} \left(\boldsymbol{D}^{cr} \right)^{-1} \left(\boldsymbol{T}^{cr} \right) \right] \right\}^{-1} \Delta\boldsymbol{\varepsilon} \tag{5.56}$$

or

$$\Delta\boldsymbol{\sigma} = \boldsymbol{D}^{crco} \Delta\boldsymbol{\varepsilon} \tag{5.57}$$

where $\boldsymbol{D}^{crco}$ is the constitutive matrix for the cracked material state:

$$\boldsymbol{D}^{crco} = \left\{ \left(\boldsymbol{D}^{co} \right)^{-1} + \sum_{i=1}^{Ncrack} \left[\left(\boldsymbol{T}^{cr} \right)^{T} \left(\boldsymbol{D}^{cr} \right)^{-1} \left(\boldsymbol{T}^{cr} \right) \right] \right\}^{-1} \tag{5.58}$$

5.3.3 Crack fracture parameters

The crack constitutive matrix $\boldsymbol{D}^{cr}$ distinguishes between mode I and mode II failure and it is assumed that there is no interaction between these two modes. This means that coupling among normal and shear components in the crack traction-strain expressions are neglected [Lotfi and Espandar 2004]. The $\boldsymbol{D}^{cr}$ matrix is defined diagonal as:

$$\boldsymbol{D}^{cr} = \begin{bmatrix} D_I^{cr} & 0 \\ 0 & D_{II}^{cr} \end{bmatrix} \tag{5.59}$$

where D_I^{cr} and D_{II}^{cr} are the mode I and mode II stiffness modulus associated with the crack behaviour.

Mode I stiffness is given by:

$$D_I^{cr} = -\frac{\alpha_2 \cdot f_t^2 \cdot h}{2G_f^I} \tag{5.60}$$

where f_t is the tensile strength, G_f^I is the fracture energy release rate, which are material constants, α_2 is a parameter that depends on the shape of the softening curve [Lotfi and Espandar 2004], h is the characteristic length related to mesh size [Bažant and Oh 1983]. When using a 4-nodes shell element, h is taken as the square root of the area of the finite element. For 8-node element, h is half of the previous value. When using a solid, h is the diagonal of the volume.

To avoid snap-back instability, the characteristic length is subjected to the following constraint [de Borst 1991]:

$$h \leq \frac{G_f \cdot E_c}{b \cdot f_t^2} \tag{5.61}$$

where b depends to the shape of the softening curve.

The crack interface shear stiffness D_{II}^{cr} is expressed in terms of uncracked material shear modulus G as:

$$D_{II}^{cr} = \frac{\beta_t}{1-\beta_t} G \tag{5.62}$$

where β_t is the shear retention factor. A value of 0.1 is suggested by Lotfi and Espandar [2004]. According to Rots [1988], β_t can be written as:

$$\beta_t = \left(1 - \frac{\varepsilon_n^{cr}}{\varepsilon_{n,ult}^{cr}}\right)^{p_1} \tag{5.63}$$

5.4 SMEARED CRACK MODEL: TOTAL-STRAIN MODEL

In this model the stress is assumed to be a function of the total strain [Feenstra and Rots 2001]. This model is divided in a fixed orthogonal crack model or a coaxial rotating crack model, depending on the approach to the shear stress-strain relation. The constitutive relationships can be described in terms of the tension and compression stress-strain relations. When the material enters in the inelastic region, the cracking only influences the diagonal terms in the compliance matrix $\boldsymbol{D}^c$, as specified by Feenstra and de Borst [1992]. In the local coordinate system the total stress-strain relation in plane-stress is:

$$\boldsymbol{\sigma}_l^c = \boldsymbol{D}^c \, \boldsymbol{\varepsilon}_l^c = \begin{bmatrix} \dfrac{\alpha_n E}{1-\alpha_n \alpha_t \upsilon^2} & \dfrac{\alpha_t \alpha_n E}{1-\alpha_n \alpha_t \upsilon^2} & 0 \\ \dfrac{\alpha_n \alpha_t E}{1-\alpha_n \alpha_t \upsilon^2} & \dfrac{\alpha_t E}{1-\alpha_n \alpha_t \upsilon^2} & 0 \\ 0 & 0 & \beta_t G \end{bmatrix} \boldsymbol{\varepsilon}_l^c \tag{5.64}$$

where α_n and α_t are reduction factors for the elasticity modulus and are only functions of the tensile strains in the considered directions, β_t is the shear retention factor. In the global coordinate system the previous equation is re-written using the strain transformation matrix $\boldsymbol{T}^c$ that is equal to $\boldsymbol{T}^{cr}$, resulting in:

$$\boldsymbol{\sigma} = \left[\left(\boldsymbol{T}^{c} \right)^{T} \boldsymbol{D}^{c} \left(\boldsymbol{T}^{c} \right) \right] \boldsymbol{\varepsilon} \tag{5.65}$$

In case of uploading, the model tends to point towards the origin in the stress-strain curve (Figure 5.14). This is achieved by introducing a stiffness degradation unloading constraint r_k computed for both tension and compression zones individually [Midas FEA v2.9.6 2009].

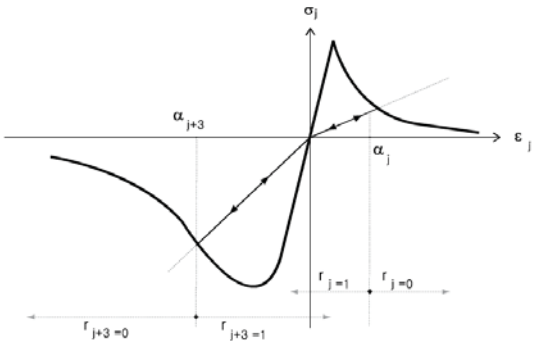

Figure 5.14.Loading and unloading behaviour of the Total Strain Crack model [Midas FEA v2.9.6 2009].

5.4.1 Compressive behaviour with lateral cracking

When the material is cracked, lateral tensile strains perpendicular to the principal compressive direction reduces the compressive strength. Due to lateral confinement the compressive stress-strain relationship is modified to incorporate the effects of increased isotropic stress and lateral confinement. The concept of failure function is introduced to compute the compressive stress, which causes failure as a function of the confining stress in the lateral directions. If the material is cracked in the lateral directions, the peak compressive stress is reduced by $\beta_{\sigma,cr}$ and the strain at peak compressive stress by $\beta_{\varepsilon,cr}$. This reduction factors was proposed by Vecchio and Collins [1986].

$$f_p = \beta_{\sigma,cr} \cdot f_c \qquad \alpha_p = \beta_{\varepsilon,cr} \cdot \varepsilon_p \tag{5.66}$$

5.5 DAMAGED PLASTICITY MODEL

The plastic-damage model is based on the work by Lubliner *et al.* [1989] and by Lee and Fenves [1998]. This model is a continuum, plastic-based, damage model originally developed for concrete, where the two main failure mechanisms are tensile cracking and compressive crushing of the material. This model assumes that material failure can be effectively modelled using its uniaxial tension, uniaxial compression and plasticity characteristics. The cracking in the material model is represented by the damage factors

that reduce the elasticity modulus in tension and compression (Figure 5.15). Contrary to the classical theory of plasticity, the damaged plasticity model uses a set of variables that alters the elastic and plastic behaviour.

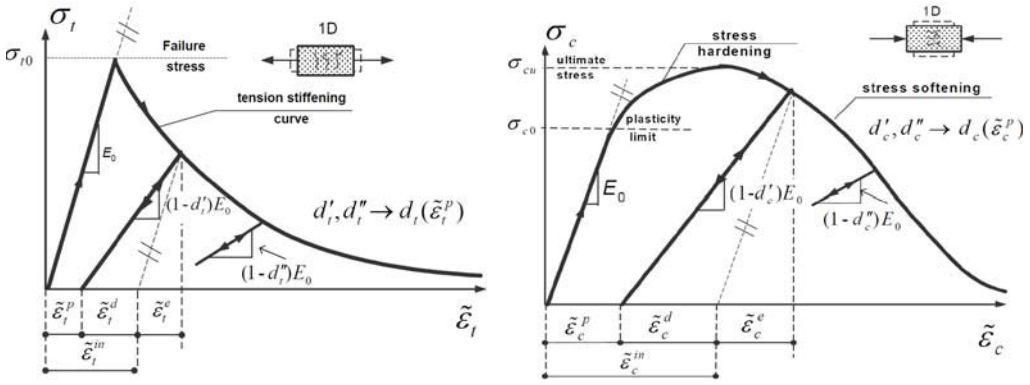

a) Tension behaviour **b) Compression behaviour**

Figure 5.15. Response of concrete under compression and tension loads implemented in Abaqus for the damaged plasticity model (modified from Wawrzynek and Cincio [2005]).

The yield surface is controlled by two hardening variables: the tensile equivalent plastic strain, $\tilde{\varepsilon}_t^{pl}$, and the compressive equivalent plastic strain, $\tilde{\varepsilon}_c^{pl}$, linked to the tension and compression failures respectively. The equivalent plastic strains are equal to the total strains minus the elastic strains.

5.5.1 Strain rate decomposition

In the incremental theory of plasticity, the total strain rate $\dot{\varepsilon}$ is decomposed into an elastic part and a plastic part as shown in Equation (5.1) and repeated here for convenience:

$$\dot{\varepsilon} = \dot{\varepsilon}^{el} + \dot{\varepsilon}^{pl} \tag{5.67}$$

where $\dot{\varepsilon}^{el}$ is the elastic part of the strain rate, and $\dot{\varepsilon}^{pl}$ is the plastic strain rate. The plastic strain represents all irreversible deformations including those caused by micro-cracks.

5.5.2 Stress-strain relations

The stress-strain relation is:

$$\boldsymbol{\sigma} = \left(1-d\right)\boldsymbol{D}_0^{el} \cdot \left(\varepsilon - \varepsilon^{pl}\right) = \boldsymbol{D}^{el} \cdot \left(\varepsilon - \varepsilon^{pl}\right) \tag{5.68}$$

where $\boldsymbol{D}_0^{el}$ is the undamaged elastic stiffness of the material, $\boldsymbol{D}^{el}$ represents the degraded elastic stiffness. The damage variable d ranges from 0 (no damage) to 1(complete loss of integrity), the total strain is represented by $\boldsymbol{\varepsilon}$, and the plastic strain by $\boldsymbol{\varepsilon}^{pl}$.

According to Malm [2009], in case of proportional loading of concrete structures, where cracking results from uniaxial tensile stress, isotropic models are considered sufficiently accurate. The stiffness degradation is isotropic and characterized by a single degradation variable d . In continuum damage mechanics, the stiffness degradation (or damage variable) can be modelled by defining a relation between Cauchy stresses and effective stresses as follows:

$$\bar{\boldsymbol{\sigma}} = \frac{\boldsymbol{\sigma}}{(1-d)} \tag{5.69}$$

where $\bar{\sigma}$ is the effective stress.

Substituting Equation (5.69) into Equation (5.68):

$$\bar{\boldsymbol{\sigma}} = \boldsymbol{D}_0^{el} \cdot \left(\varepsilon - \varepsilon^{pl}\right) \tag{5.70}$$

When damage occurs, the effective stress is more representative than the Cauchy stress because it is the effective stress area that carries the external loads [Abaqus 6.9 SIMULIA 2009].

5.5.3 Hardening variables

Two hardening variables are used to characterize damage states in tension and compression.

$$\tilde{\varepsilon}^{pl} = \begin{bmatrix} \tilde{\varepsilon}_t^{pl} \\ \tilde{\varepsilon}_c^{pl} \end{bmatrix} \tag{5.71}$$

$\tilde{\varepsilon}_t^{pl}$ and $\tilde{\varepsilon}_c^{pl}$ refer to equivalent plastic strains in tension and compression, respectively. These variables control the evolution of the yield surface and the degradation of the elastic stiffness. The evolution of the hardening variables is given by:

$$\dot{\tilde{\varepsilon}}^{pl} = \boldsymbol{h}\left(\bar{\boldsymbol{\sigma}}, \tilde{\varepsilon}^{pl}\right) \cdot \dot{\varepsilon}^{pl} \tag{5.72}$$

$$\tilde{\varepsilon}_t^{pl} = \int_0^t \dot{\tilde{\varepsilon}}_t^{pl}\, dt \tag{5.73}$$

$$\tilde{\varepsilon}_c^{pl} = \int_0^t \dot{\tilde{\varepsilon}}_c^{pl}\, dt \tag{5.74}$$

5.5.4 Yield function

The plastic damaged concrete model in Abaqus make uses of the yield function proposed by Lubliner *et al.* [1989] and incorporates the modifications proposed by Lee and Fenves [1998] to account for different strength evolution under tension and compression.

The yield function uses two stress invariants of the effective stress tensor: the effective hydrostatic pressure, $\overline{p}$, and the Mises equivalent effective stress, $\overline{q}$. Its evolution is controlled by the hardening variables $\tilde{\varepsilon}_t^{pl}$ and $\tilde{\varepsilon}_c^{pl}$.

The two stress invariants are defined as:

$$\overline{p} = -\frac{1}{3}\overline{\boldsymbol{\sigma}} \cdot \boldsymbol{I} \tag{5.75}$$

$$\overline{q} = \sqrt{\frac{3}{2}\overline{\boldsymbol{S}} \cdot \overline{\boldsymbol{S}}} \tag{5.76}$$

where $\overline{\boldsymbol{S}}$ represents the deviatoric part of the effective stress tensor $\overline{\boldsymbol{\sigma}}$, defined as:

$$\overline{\boldsymbol{S}} = \overline{p}\boldsymbol{I} + \overline{\boldsymbol{\sigma}} \tag{5.77}$$

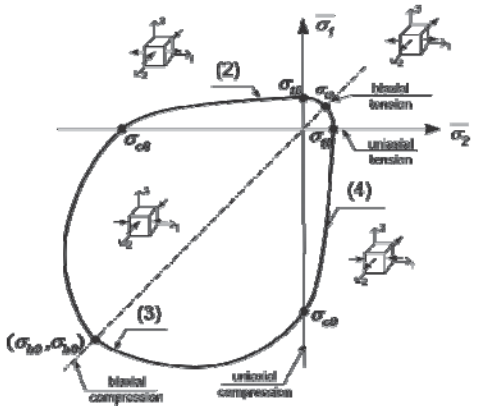

Figure 5.16. Yield surface for the plane stress space (modified from Wawrzynek and Cincio [2005]).

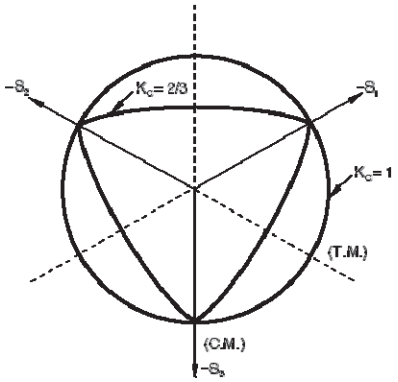

Figure 5.17. Yield surface in the deviatoric plane corresponding to different values of Kc [Abaqus 6.9 SIMULIA 2009].

The yield function (represented in Figure 5.16 and Figure 5.17) is expressed as:

$$F\left(\bar{\sigma},\tilde{\varepsilon}^{pl}\right)=\frac{1}{1-\alpha}\left(\bar{q}-3\alpha\,\bar{p}+\beta\left(\tilde{\varepsilon}^{pl}\right)\left\langle\hat{\bar{\sigma}}_{\max}\right\rangle-\gamma\left\langle-\hat{\bar{\sigma}}_{\max}\right\rangle\right)-\bar{\sigma}_c\left(\tilde{\varepsilon}_c^{pl}\right)\leq 0 \tag{5.78}$$

with

$$\alpha=\frac{\sigma_{b0}-\sigma_{c0}}{2\sigma_{b0}-\sigma_{c0}} \tag{5.79}$$

$$\beta=\frac{\bar{\sigma}_c\left(\tilde{\varepsilon}_c^{pl}\right)}{\bar{\sigma}_t\left(\tilde{\varepsilon}_t^{pl}\right)}\left(1-\alpha\right)-\left(1+\alpha\right) \tag{5.80}$$

$$\gamma=\frac{3\left(1-K_c\right)}{2K_c-1} \tag{5.81}$$

where α and γ are dimensionless material constants, $\hat{\bar{\sigma}}_{\max}$ is the algebraically maximum principal effective stress, $\bar{\sigma}_t$ and $\bar{\sigma}_c$ are the effective tension and compressive cohesion stress, σ_{b0} is the initial equibiaxial compressive yield stress, σ_{c0} is the initial uniaxial compressive yield stress. K_c is the ratio of the second stress invariant on the tensile meridian, $q_{(TM)}$, to that on the compressive meridian, $q_{(CM)}$, at initial yield for any given value of pressure invariant p such that the maximum principal stress is negative: $\hat{\bar{\sigma}}_{\max}<0$. A value of $K_c=2/3$ is recommended for concrete [Lubliner *et al.* 1989].

The concrete damage plasticity model assumes a non associated plastic flow rule given by:

$$\dot{\varepsilon}^{pl} = \dot{\lambda} \frac{\partial G(\bar{\boldsymbol{\sigma}})}{\partial \bar{\boldsymbol{\sigma}}} \tag{5.82}$$

where $\dot{\lambda}$ is the nonnegative plastic multiplier. The flow potential G represents the Drucker-Praguer hyperbolic function:

$$G = \sqrt{\left(e \cdot \sigma_{t0} \cdot \tan\psi\right)^2 + \bar{q}^2} - \bar{p} \cdot \tan\psi \tag{5.83}$$

where e is a parameter, referred to as the eccentricity, that defines the rate at which the function approaches the asymptote (the flow potential tends to a straight line as the eccentricity tends to zero); σ_{t0} is the uniaxial tensile stress at failure; and ψ is the dilatation angle measured in the $p-q$ plane at high confining pressures. A low value of dilatancy is recommended for quasi-brittle materials [Malm 2009].

The recommended value for the eccentricity is $e = 0.1$, which implies that the material has almost the same dilatation angle over a wide range of confining pressure stress values [Abaqus 6.9 SIMULIA 2009].

5.5.5 Damage and stiffness degradation under uniaxial condition

5.5.5.1 *Uniaxial behaviour*

The uniaxial tensile and compressive response of concrete/masonry is characterized by damage plasticity. The stress-strain curves are also converted into stress versus plastic strain curves of the form:

$$\sigma_t = \sigma_t\left(\tilde{\varepsilon}_t^{pl}, \dot{\tilde{\varepsilon}}_t^{pl}, \theta, f_i\right) \tag{5.84}$$

$$\sigma_c = \sigma_c\left(\tilde{\varepsilon}_c^{pl}, \dot{\tilde{\varepsilon}}_c^{pl}, \theta, f_i\right) \tag{5.85}$$

where $\tilde{\varepsilon}_t^{pl}$ and $\tilde{\varepsilon}_c^{pl}$ are the equivalent plastic strains, $\dot{\tilde{\varepsilon}}_t^{pl}$ and $\dot{\tilde{\varepsilon}}_c^{pl}$ are the equivalent plastic strain rates, θ is the temperature, and f_i are other predefined field variables.

Figure 5.15a shows the tensile behaviour of the material, the elastic part is linear up to the failure stress σ_{t0}. The failure corresponds to the onset of micro-cracking in the material. After this point, the formation of micro-cracks is represented macroscopically by softening stress-strain response. Under compression behaviour (Figure 5.15b), the material behaves linearly until the initial yield stress, σ_{c0}. Thereafter, the material is characterized by stress hardening and stress softening after reaching the ultimate stress, σ_{cu}. When the specimen is unloaded from any part of the softening branch of the stress-

strain curves, the unloading response degrades as seen in Figure 5.15. The degradation of the elastic stiffness $\boldsymbol{D}$ is characterized by two uniaxial damage variables, d_c and d_t, expressed as:

$$d_t = d_t\left(\tilde{\varepsilon}_t^{pl}, \theta, f_i\right), \ \left(0 \le d_t \le 1\right) \tag{5.86}$$

$$d_c = d_c\left(\tilde{\varepsilon}_c^{pl}, \theta, f_i\right), \ \left(0 \le d_c \le 1\right) \tag{5.87}$$

where $\tilde{\varepsilon}_t^{pl}$ and $\tilde{\varepsilon}_c^{pl}$ are the equivalent plastic strain, θ is the temperature, and f_i are other predefined field variables. The damage variables range from zero (no damaged material) until 1 (complete damaged material).

Considering the damaged variables, the stress-strain relationships are formulated as:

$$\sigma_t = \left(1 - d_t\right) E_0 \left(\varepsilon_t - \tilde{\varepsilon}_t^{pl}\right) \tag{5.88}$$

$$\sigma_c = \left(1 - d_c\right) E_0 \left(\varepsilon_c - \tilde{\varepsilon}_c^{pl}\right) \tag{5.89}$$

The effective uniaxial cohesion stresses determine the size of the yield surface and are given as:

$$\bar{\sigma}_t = \frac{\sigma_t}{\left(1 - d_t\right)} = E_0 \left(\varepsilon_t - \tilde{\varepsilon}_t^{pl}\right) \tag{5.90}$$

$$\bar{\sigma}_c = \frac{\sigma_c}{\left(1 - d_c\right)} = E_0 \left(\varepsilon_c - \tilde{\varepsilon}_c^{pl}\right) \tag{5.91}$$

Under uniaxial conditions the equivalent plastic strain rates are given as $\dot{\tilde{\varepsilon}}_t^{pl} = \dot{\varepsilon}_{11}^{pl}$ for tension, and $\dot{\tilde{\varepsilon}}_c^{pl} = -\dot{\varepsilon}_{11}^{pl}$ for compression.

5.5.5.2 *Uniaxial cyclic behaviour*

Figure 5.18 shows a uniaxial load cycle of the damaged material.

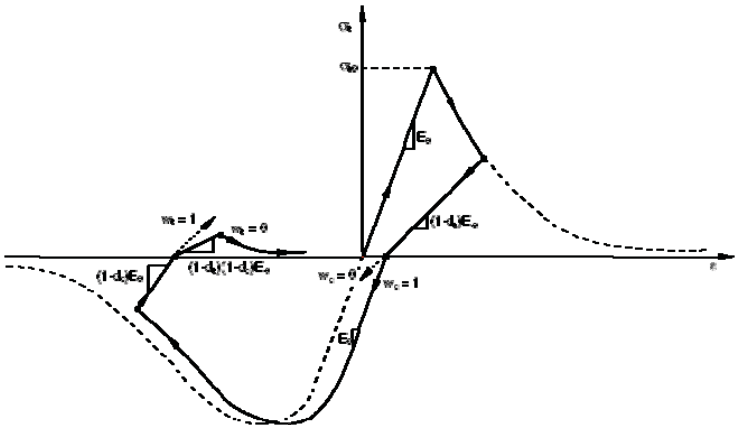

Figure 5.18. Uniaxial load cycle behaviour for the damaged plasticity model in Abaqus 6.9 SIMULIA [2009].

The reduction of the elastic modulus is given in terms of a scalar degradation variable d:

$$E=(1-d)E_0 \tag{5.92}$$

where E_0 is the material initial elasticity modulus.

The degradation variable d is a function of the stress state and the uniaxial damage variables d_t and d_c, as follows:

$$(1-d)=(1-s_t d_c)(1-s_c d_t), \qquad 0\le s_t, s_c \le 1 \tag{5.93}$$

where s_t and s_c are functions of the stress state that represents the stiffness recovery for reversal loads, expressed as:

$$\begin{aligned} s_t &= 1-w_t r^*(\bar{\sigma}_{11}), && 0\le w_t \le 1 \\ s_c &= 1-w_c\left(1-r^*(\bar{\sigma}_{11})\right), && 0\le w_c \le 1 \end{aligned} \tag{5.94}$$

where w_t and w_c are factors that control the recovery of the tension and compression stiffness upon load reversal, and $r^*(\bar{\sigma}_{11})$ is a function of the tensile $(\bar{\sigma}_{11}>0)$ and compressive $(\bar{\sigma}_{11}<0)$ side of the cycle, defined as:

$$r^*(\bar{\sigma}_{11})=H(\bar{\sigma}_{11})=\begin{cases} 1 & if\ \ \bar{\sigma}_{11}>0 \\ 0 & if\ \ \bar{\sigma}_{11}<0 \end{cases} \tag{5.95}$$

Figure 5.19 shows the effect of the recovery factors when the load changes from tension to compression. The initial stiffness in compression is full recovered when $w_c = 1$ and there is no stiffness recovery when $w_c = 0$. Under uniaxial cyclic conditions the equivalent plastic strain are also generalized as $\dot{\tilde{\varepsilon}}_t^{pl} = r^* \dot{\varepsilon}_{11}^{pl}$ in tension, and $\dot{\tilde{\varepsilon}}_c^{pl} = -\left(1 - r^*\right)\dot{\varepsilon}_{11}^{pl}$ in compression.

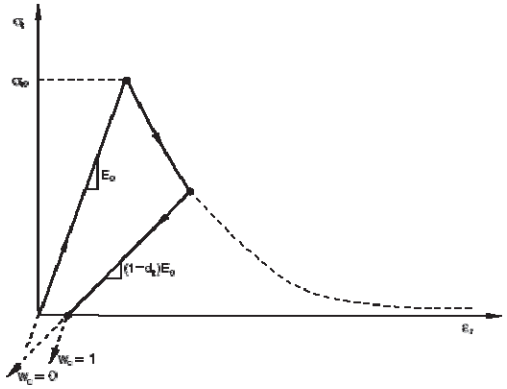

Figure 5.19. Effect of the compression recovery parameter w_c [Abaqus 6.9 SIMULIA 2009].

5.5.5.3 *Multiaxial conditions*

The stress-strain relationships for the general three-dimensional multiaxial conditions are given by the scalar damage elasticity equation:

$$\boldsymbol{\sigma} = \boldsymbol{D}^{el} \cdot \left(\varepsilon - \varepsilon^{pl}\right) \tag{5.96}$$

where $\boldsymbol{D}^{el}$ is the damaged elasticity matrix defined as:

$$\boldsymbol{D}^{el} = \left(1 - d\right)\boldsymbol{D}_0^{el} \tag{5.97}$$

For the evaluation of the scalar stiffness degradation d, the function $r^*\left(\bar{\sigma}_{11}\right)$ is updated with the multiaxial stress weight factor $r\left(\hat{\boldsymbol{\sigma}}\right)$, defined as:

$$r\left(\hat{\bar{\boldsymbol{\sigma}}}\right) = \frac{\sum_{i=1}^{3}\left\langle \hat{\bar{\sigma}}_i \right\rangle}{\sum_{i=1}^{3}\left|\hat{\bar{\sigma}}_i\right|},\ 0 \le r\left(\hat{\bar{\boldsymbol{\sigma}}}\right) \le 1 \tag{5.98}$$

where $\hat{\sigma}_i \ \ (i=1,2,3)$ are the principal stress components. The Macaulay bracket $\langle\cdot\rangle$ is defines by $\langle x\rangle = \frac{1}{2}\left(|x|+x\right)$.

Under multiaxial conditions the equivalent plastic strain rates are evaluated by $\dot{\tilde{\varepsilon}}_t^{pl} = r\left(\hat{\boldsymbol{\sigma}}\right)\dot{\hat{\varepsilon}}_{\max}^{pl}$ in tension, and $\dot{\tilde{\varepsilon}}_c^{pl} = -\left(1-r\left(\hat{\boldsymbol{\sigma}}\right)\right)\dot{\hat{\varepsilon}}_{\min}^{pl}$ in compression.

5.6 COMPRESSION AND TENSION CONSTITUTIVE LAWS

5.6.1 Compression models

In this work, a parabolic compression curve has been selected for modelling the adobe material (Figure 5.20). The function parameters are defined by Lourenço [1996] assuming a hardening-softening behaviour in compression, where the fracture energy is represented by G_f^c. Equation (5.99) allow to compute the compression curve.

$$\begin{aligned}
\bar{\sigma}_a\left(k_3\right) &= \bar{\sigma}_i + \left(\bar{\sigma}_p - \bar{\sigma}_c\right)\sqrt{\frac{2k_3}{k_p} - \frac{k_3^2}{k_p^2}} \\
\bar{\sigma}_b\left(k_3\right) &= \bar{\sigma}_p + \left(\bar{\sigma}_m - \bar{\sigma}_p\right)\left(\frac{k_3 - k_p}{k_m - k_p}\right)^2 \\
\bar{\sigma}_c\left(k_3\right) &= \bar{\sigma}_r + \left(\bar{\sigma}_m - \bar{\sigma}_r\right)\exp\left(m\frac{k_3 - k_m}{\bar{\sigma}_3 - \bar{\sigma}_r}\right)
\end{aligned} \tag{5.99}$$

with $m = 2\dfrac{\bar{\sigma}_m - \bar{\sigma}_p}{k_m - k_p}$.

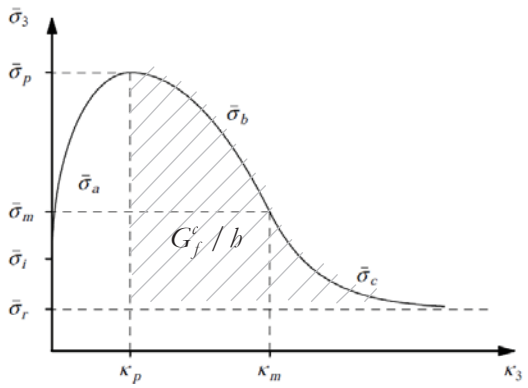

Figure 5.20. Parabolic compression curve used for modelling masonry material.

5.6.2 Tension models

The softening behaviour in a tensile constitutive law is represented by the fracture energy G_f^I. Figure 5.21 shows different curves for the stress-strain relation. The model used to characterize the adobe material is based on an exponential softening, similar to the one used by Lourenço [1998] for masonry. The stress in the softening region is given by:

$$\sigma_{nn}^{cr} = f_t \exp\left(-\frac{f_t}{G_f^I}\varepsilon_{nn}^{cr}\right) \tag{5.100}$$

where f_t is the maximum tensile strength, G_f^I is the fracture energy and ε_{nn}^{cr} is the crack strain.

The Mode I fracture energy G_f^I is related to the equivalent length or crack bandwidth, h, through Equation (5.101).

$$G_f^I = h\int_0^{\infty} \sigma_{nn}^{cr}\left(\varepsilon_{nn}^{cr}\right) d\varepsilon_{nn}^{cr} \tag{5.101}$$

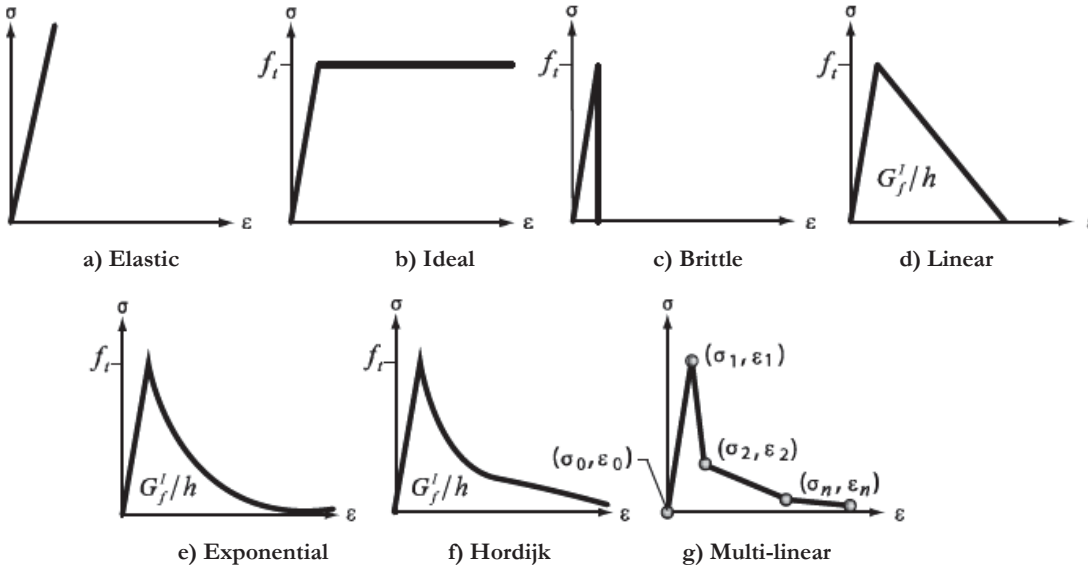

a) Elastic b) Ideal c) Brittle d) Linear

e) Exponential f) Hordijk g) Multi-linear

Figure 5.21. Tension models.

5.7 SUMMARY

The numerical modelling of cracking and damage in concrete/masonry panels is based on discrete mechanics and continuum mechanics, and that plasticity based models are suitable for micro and macro modelling of masonry. In this chapter, a review of the theory of plasticity as well as a description of the formulation for discrete (*i.e.* fracture mechanics) and continuum models are given.

For the discrete model the combined cracking-shearing-crushing model is given here. For the continuum model two approaches are described: the smear crack approach and a damage plasticity based model. These models are going to be used in the following chapters with two finite element programmes: Midas FEA and Abaqus. Unlike smeared crack models, the damaged plasticity model represents the cracking behaviour by damage factors that modify the constitutive laws for unloading.

Two formulations of the smeared crack models are discussed: decomposed-strain model and total-strain model. The first one separates the elastic and crack strain for computing stress levels, while the second one makes used of the total material strain for computing stress levels at the integration points.

Finally, constitutive laws for representation of tension and compression behaviour are reported. In this work, the compression of adobe masonry in the inelastic range is represented by a parabolic function and the tension by an exponential function. The inelastic material parameters for adobe masonry are shown in the next chapter.

page intentionally left blank.